HELSINKI UNIVERSITY OF TECHNOLOGY
Faculty of Chemistry and Materials Sciences
Degree Programme of Forest Products Technology

Juuso Rantanen

CONSTRUCTION OF A SINGLE BAR REFINER

Master's Thesis for the degree of Master of Science in Technology submitted for inspection, Espoo, 22 December 2009.

Supervisor   Professor Hannu Paulapuro

Instructor   Eero Hiltunen, D.Sc. (Tech)

HELSINKI UNIVERSITY OF TECHNOLOGY
Faculty of Chemistry and Materials Sciences
Degree Programme: Forest Products Technology

ABSTRACT OF MASTER'S THESIS

Author **Juuso Rantanen**	
Title of Thesis **Construction of a Single Bar Refiner**	

Abstract

The target of this thesis work was to construct a laboratory scale low-consistency refiner by modifying an existing design to enable more realistic refining conditions. The aim of the modification was to be able to study refining energy and forces affecting fibres more closely, particularly enabling the determination of bar coverage and pulp consistency in the gap by image analysis. The designing and construction of a pulp flow system for the refiner unit was also an important part of the thesis. Setup and testing of a system for imaging fibres in the refining gap was realized.

The modification of the original design was made by designing a new stator bar with dimensions similar to the rotor bar. The purpose of this design was to create more realistic conditions during refining. This design was first tested with the original stator bar by machining it with a groove similar to the one in the rotor bar, and later constructing two additional bars to reach the desired smaller gap size. The pulp flow system was designed and constructed to enable even flow conditions for the refiner unit. The installing and setup of the laser illuminated imaging system was conducted to enable image capture of the refining phenomena.

Some problems were encountered during the course of this work. The errors in measuring the original gap size resulted in wrong dimensioning of the new stator parts. For this reason some modifications had to be made afterwards to reach the targeted gap sizes. The pulp flow system was constructed without any major issues, but problems with the refiner unit clogging when operating with pulp consistencies > 2 % left some room for improvement. The imaging system installation and preliminary trials were successful, resulting in some good images from the gap between the rotor and stator bars. Images showed e.g. that bar coverage is clearly not 100 % at 2 % pulp consistency with 150 μm gap size, and that there is potential in developing the image analysis method aiming to determine bar coverage and pulp consistency in the gap. The target of the thesis to construct a research tool for refining studies was achieved

Tekijä
Juuso Rantanen

Diplomityön nimi
Yksiteräjauhimen rakentaminen

Tiivistelmä

Tämän diplomityön tavoitteena oli rakentaa laboratoriomittakaavan jauhin matalasakeusjauhatuksen ilmiöiden tutkimista varten muokkaamalla jo olemassa olevan jauhimen terärakennetta vastaamaan todenmukaisemmin oikeita teräolosuhteita. Muokkauksen tavoite oli kyetä tutkimaan jauhatusenergiaa ja kuituihin vaikuttavia voimia. Erityisesti tavoitteena oli mahdollistaa parametrien, kuten massan terävälisakeus ja terän peittävyys, määrittäminen kuva-analyysin avulla. Jauhimen massakierron suunnittelu ja rakentaminen, sekä kuvauslaitteiston asennus ja testaus olivat myös osa työtä.

Alkuperäistä terärakennetta muokattiin siten, että staattoriterän dimensiot saatiin identtisiksi roottoriterän kanssa. Tämän rakenteen tavoitteena oli saada jauhatusolosuhteet vastaamaan enemmän todellisia jauhatusolosuhteita. Uutta rakennetta testattiin ensin koneistamalla vanha staattoriterä, ja myöhemmin suunnittelemalla kaksi uutta terää, jotta teräväli saatiin pienemmäksi ja näin vastaamaan paremmin todellista jauhatustilannetta. Massakierron suunnittelun ja rakentamisen tavoitteena oli luoda jauhimelle tasaiset virtausolosuhteet, ja laservalaistun kuvauslaitteiston asennuksen tarkoituksena oli mahdollistaa jauhatustapahtumien kuvaus terävälistä.

Staattoriterien suunnittelussa ja valmistamisessa esiintyi joitakin ongelmia, erityisesti virhe alkuperäisen terävälin mittaamisessa johti siihen, että uusien terien mitoitukseen tuli virhe. Tämä onnistuttiin kuitenkin korjaamaan pienillä muutoksilla terien rakenteeseen. Massakierron rakentamisessa ei esiintynyt suuria ongelmia, mutta sakeuden nostaminen yli 2 %:iin johti usein jauhimen tukkeutumiseen, joten sitä korkeampiin sakeuksiin ei toistaiseksi päästy. Kuvauslaitteiston asentaminen ja alustavat kokeet olivat menestyksekkäitä, ja tuloksena oli hyvälaatuisia kuvia terävälistä. Kuvista voitiin mm. päätellä, että terä ei peity kokonaisuudessaan massalla 2 % sakeudessa 150 µm terävälillä. Alustavien kokeiden perusteella kuva-analyysin kehittäminen massan sakeuden ja terän peittävyyden määrittämiseksi on mahdollista. Diplomityön tavoite toimivan jauhatustutkimuslaitteen rakentamiseksi saavutettiin.

ACKNOWLEDGEMENTS

TABLE OF CONTENTS

1 INTRODUCTION

Beating or refining of chemical pulp has been used by papermakers to introduce better papermaking quality for the final product. Untreated chemical pulp fibers have low tendency of bonding and flexibility which may result in low paper strength properties. Also the formation of sheets can be uneven due to high flocculation of pulp fibres /1/.

Refining of chemical pulp is one of the most researched areas in papermaking and much progress has been already made. Despite this fact there still remain some areas and phenomena that are not fully understood. Earlier studies have been focusing mostly on changes produced in pulp and their effect on paper quality, for example internal and external fibrillation, fibre shortening and secondary fines production /2, 3/. Refining energy and especially forces that eventually create these changes have not been studied as thoroughly, hence the need for this project.

The target of this thesis was to construct a laboratory scale refiner for chemical pulp (Single Bar Refiner, SBR) to study the refining forces and phenomena itself more closely. The specific objective was to enable determination of fractional bar coverage and pulp consistency in the gap. A first version of SBR was already built as part of an earlier project in which TKK Paper and Printing technology group had a significant contribution /4/. However, some changes on the design of the SBR were proposed to get a better and more realistic understanding of the mechanics of chemical pulp refining.

The literature part of this thesis consists of two parts. The first part is a basic introduction on low-consistency refining of chemical pulp; history, equipment, effects on fibres etc. The second part gives an understanding about the mechanics and forces that take place between the refiner bars and within fibres. Different theories of these phenomena will also be introduced in this part. The practical part will include the design, construction and some preliminary trials with the Single Bar Refiner.

2 HISTORY OF REFINING

The term "beating" originates from early papermaking history when wet rag fibres were manually beaten to disintegrate them and create bonding surfaces. Nowadays papermakers still widely talk about beating instead of refining of chemical pulp and the term is also found in modern literature. The first mechanical refining devices were introduced during the 13th century in Italy where the stamping or hammer mills were invented (Figure 1). A battery of heavy pestles fitted with metallic surfaces was operated by a shaft that took its energy usually from a waterwheel. Rags were disintegrated to shorter fibres to better suite papermaking demands.
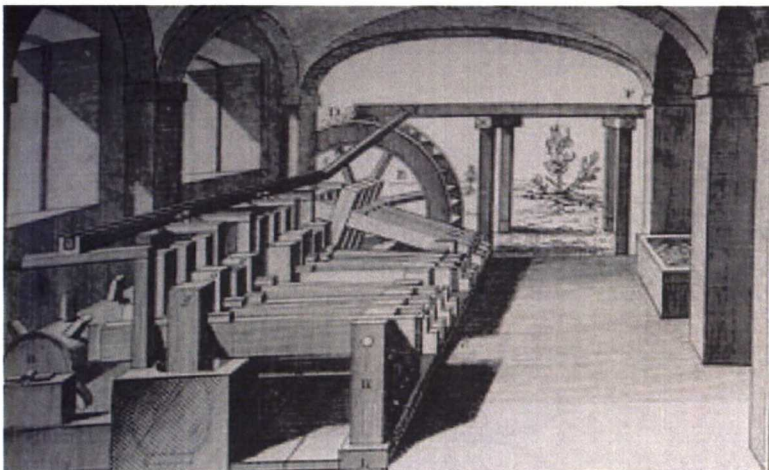
Figure 1. Hammer mills used to prepare fibres for papermaking /1/.

Later after the invention of Hollander beaters the refining process became more and more mechanized. Better formation and surface properties for end product could not be reached if the fibres from chemical pulp or cotton rags retained their original length. In Hollander beater (Figure 2) the fibres passed between rotating (rotor) and static (stator) bars that enabled fibre length reduction and other refining effects. Most of the modern day refiners are using the same principle. /5, 1/
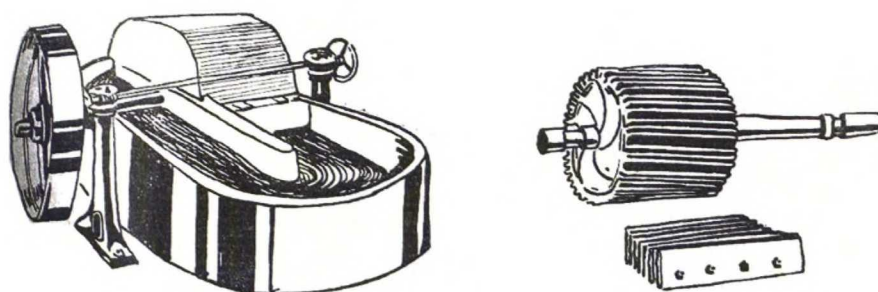
Figure 2. An early 20th century Hollander (left) with its rotor and stator bars (right) /6/.

3 EQUIPMENT

3.1 Laboratory and pilot scale refiners

3.1.1 Valley beater

Many of the laboratory scale refiners are based on similar construction as the historical Hollander beater. This is due to its simple and cost-effective design, adequate capacity for laboratory work and reliability. Perhaps the most commonly used laboratory refiner in studying basic refining phenomena is the Valley beater, also known as the Hollander beater illustrated in Figure 3. It has a rotating cylinder (rotor) with bars and 2-3 bar equipped counter bed plates as a stator. Hollander beaters are batch refiners. They are quite energy intensive but they produce a gentle and homogeneous refining result. The fact that both refining energy and refining intensity can be independently controlled is also an advantage.
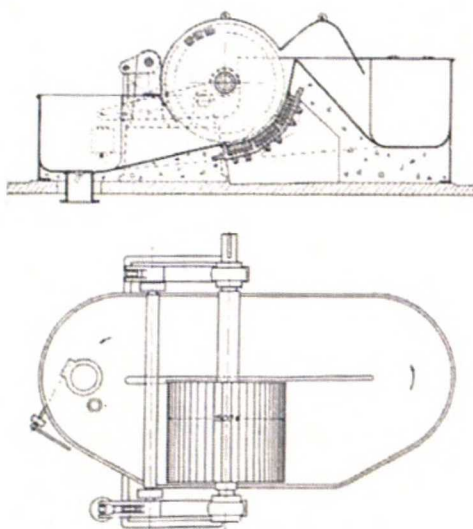
Figure 3. A schematic illustration of a Hollander beater /7/.

3.1.2 PFI-mill

The PFI-mill has become a popular laboratory refiner due to the small pulp volumes that can be used. Also the versatility of rotational direction and shear rate

are advantages. It operates in high energy and low intensity mode due to the high consistency of pulp, high shear ratio and compression forces. The refining action is created by a rotor revolving against the chamber walls. This mechanism inflicts compression and shear forces on the fibres. The working principle of the PFI-mill generates continuous fibre network redistribution which together with high pulp consistency gives a high specific energy. /8/

3.1.3 Escher-Wyss conical laboratory refiner

One of the first conical refiners that enabled laboratory refining under controlled conditions was the Escher-Wyss conical laboratory refiner, shown in Figure 4. It was developed in the 1950's specifically for laboratory purposes and later modifications have been introduced to improve the process control.
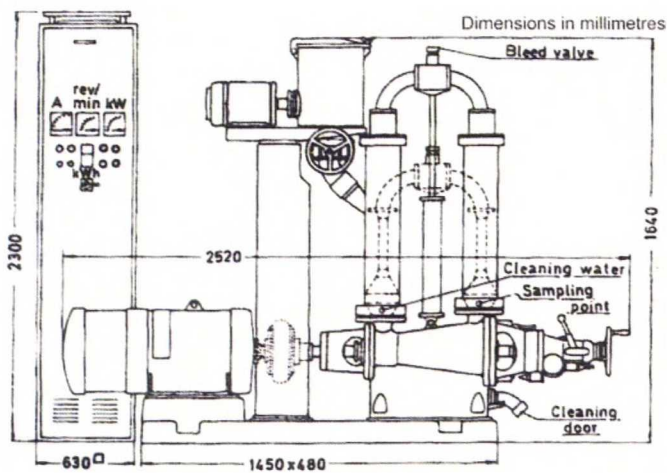
Figure 4. The Escher-Wyss conical laboratory refiner /1/.

Recent versions of the refiner can measure the refining intensity as well as calculate the specific energy based on pulp flow and power consumption. Pulp flow is controlled both by impellers at the inlet and outlet of the refiner as well as by pumping action of the fillings. Sampling is made through a specific valve that was designed to prevent settling of the pulp fibres. With conditioned fillings, the refining results are highly reproducible for a certain pulp type.

3.1.4 Voith LR 40 laboratory refiner

The LR 40 laboratory refiner by Voith has been designed to imitate production scale refining treatment as closely as possible. This means that filling design similar to that of a mill-scale refiner can be installed. The only significant difference is that the pulp passes the refining zone multiple times which may have an influence on the result. After its commissioning in 2002 a study has been made by Koskenhely /9/ concerning its reproducibility and controllability. His results indicate that with adequate warm-up time and regular checking of no-load power, measurements are reliable. Basic instrumentation and components of the LR 40 laboratory refiner are shown in Figure 5.
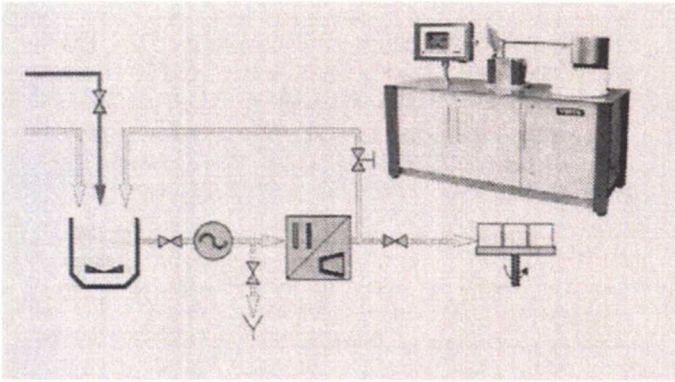
Figure 5. Basic instrumentation and mechanical parts of the laboratory refiner LR 40 /9/.

3.1.5 ProLab laboratory refiner

One of the latest inventions in laboratory refining equipment is the ProLab refining station built by Metso Paper (Figure 6). The fully automated refiner unit consists of a pulper, mixing chest, Mohno-pump, refiner housing with main motor, sampling device and appropriate piping. The refiner can be used in both disc and conical mode, and sampling is delivered automatically at predefined levels of specific energy. The ProLab refiner station is a compact solution for research and quality control purposes. Table 1 shows the technical specifications of the refiner.
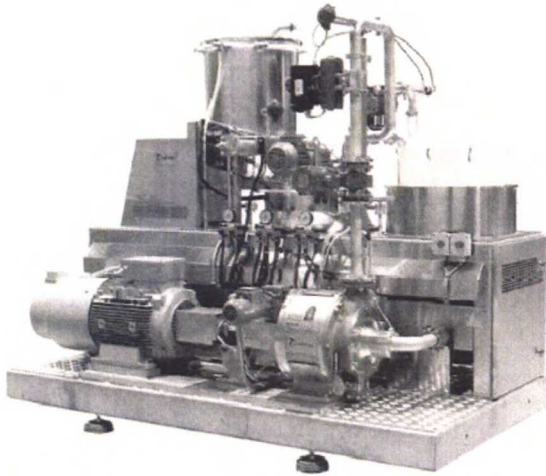
Figure 6. The ProLab laboratory refining station /1/.

Table 1. Technical specifications of the ProLab laboratory refiner /10/.

Power, kW	30
Rotor diameter, mm	
Minimum	58
Maximum	130
Pulp consistency, %	2-7
Pulp flow, L/min	50-120
Pulp feeding pressure, bar	0.5-6.0
Rotational speed, rpm	600-4500
Peripheral speed, m/s	
Minimum	5-14
Maximum	10-27
SRE/batch, kW·h/ton	10-45*
SEL, J/m	0.1-6.0*
SSL, J/m²	115-1500*

*Depending on type of fillings and pulp.

3.2 Production scale refiners

3.2.1 Introduction

Conical and disc refiners are most commonly used in mill-scale refining of chemical pulp. In both configurations pulp is fed via inlet through the refining zone and to the outlet. Refiners can have either one or two refiner zones depending on whether there are multiple stator elements. Both of these types are believed to

generate similar refining effects and they are usually controlled by the same methods. /9/

3.2.2 Jordan refiner

The first production scale conical refiner was patented by Joseph Jordan and Thomas Easton in 1858. The angle of the rotor was approximately 11-16° and the pulp consistency was around 3-4 %. Cross-section of a typical Jordan-type conical refiner is shown in Figure 7.
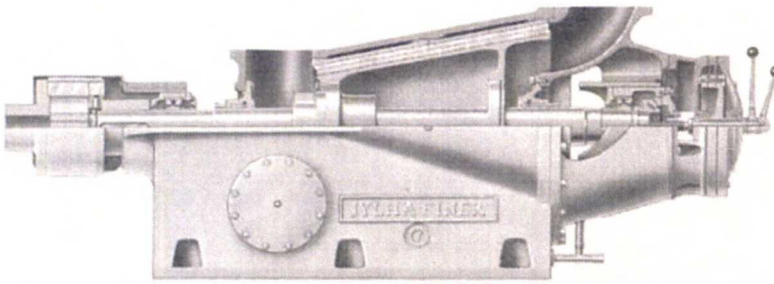
Figure 7. Cross-section of a Jordan-type refiner /7/.

The refining result was mostly fibre cutting with the traditional coarse type fillings, but when fine bars were used, the resulting fibre treatment was excellent. For this reason Jordan refiners could be used for all kinds of fibre types. However due to the size, service time requirements and low capacity, the number of these refiners has decreased. /7, 1/

3.2.3 Claflin refiner

Claflin-type conical refiner was introduced around 1920. Its construction is close to that of Jordan refiner with the differences being a wider rotor angle of about 30° and a higher peripheral speed /1/. Higher speed was probably causing less fibre shortening than with Jordan refiners. Figure 8 shows a typical Claflin-type refiner.
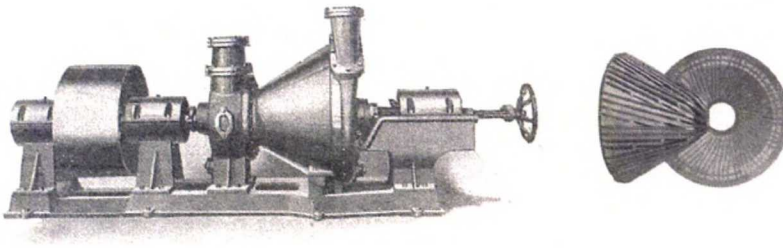
Figure 8. A Claflin refiner (left) and its typical fillings (right) /1/.

3.2.4 Modern conical refiners

Nowadays there are several suppliers for conical refiners. A common cone angle of around 20° is widely used, and other typical features like energy efficiency and high production capacity are obvious features to meet the requirements of modern papermaking. Some double- and triple-conical refiner designs are also available.

3.2.5 Disc refiners

Disc refiners can be divided into groups depending on the number of discs that are used. Single-disc refiners are used commonly in high-consistency refining because their capacity in low-consistency refining does not meet the requirements of papermaking today. Also the feeding of low-consistency pulp into a single disc refiner is difficult. J. and R. Kingsland introduced the first known disc refiner in 1856 /1/. It had one disc rotating and the other one stationary. The popularity of disc refiners started to increase when D. M. Sutherland produced the Sutherland disc refiner illustrated in Figure 9.
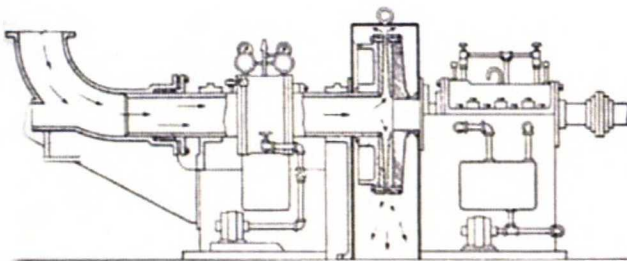
Figure 9. The design of a Sutherland disc refiner /11/.

Later, several double-disc designs based on this original refiner have been developed. In this type of design the pulp flow is divided through two refining zones formed on both sides of the rotator disc. Problem with this type of design is that the pulp flow is often split unevenly between the refining zones, which can lead to a less homogenous refining result. An example of a modern double disc refiner for low-consistency refining is shown in Figure 10.
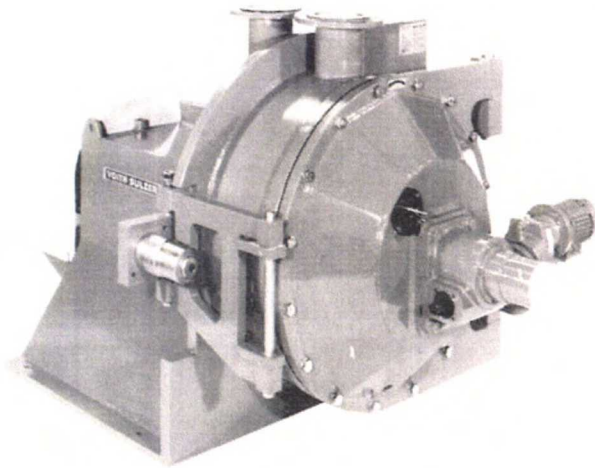
Figure 10. A Voith Sulzer Double-Disc refiner /7/.

3.3 Refiner fillings

There are several materials and material composites available for producing refiner fillings. The manufacturing process can be casting, welding, and machining or laser technology which can produce very narrow grooves and bars on the fillings. Decreasing groove and bar width has been the trend in recent decades to allow the refiner to operate with a lower calculated intensity, *SEL* and will result in having a higher cutting edge length in the refiner due to the increase in the number of bars per refiner area. /11/

Studies show that a high bar angle is more likely to promote fibrillation and a low bar angle can cause fibre cutting. This is due to the fact that fibres subjected to parallel bar edges are more likely to experience cutting effect than fibrillation. Also when refining shorter fibres a lower bar angle of about 20 ° is used com-

pared to a bar angle of about 35 ° when refining longer fibres. These angles allow the refiner to rotate in both pumping direction and non-pumping direction. /12, 11/

Sharpness of the bar edge and edges containing small-scale flaws are shown to cause severe fibre shortening. Thus the material and wear properties of the leading bar edges are also very important parameters /9/. Figure 11 shows a magnification of a low-consistency refiner bar edge.
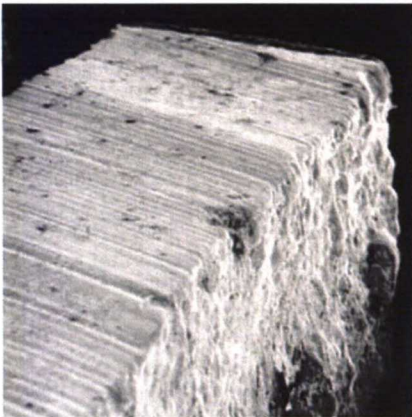
Figure 11. A magnification of a low consistency refiner bar edge /13/.

In his thesis, Koskenhely /9/ has studied the refiner gap behavior using different softwood fibre fractions (Figure 12). He concluded that at a given refining intensity, the gap of short fibre fraction (SF) was clearly narrower than that of long fibre fraction (LF). When refining unfractioned softwood kraft pulp (SWK), the gap position was usually at a value between these two fractions. These results are assumed to be because of the larger fibre flocs in longer fibre fraction.
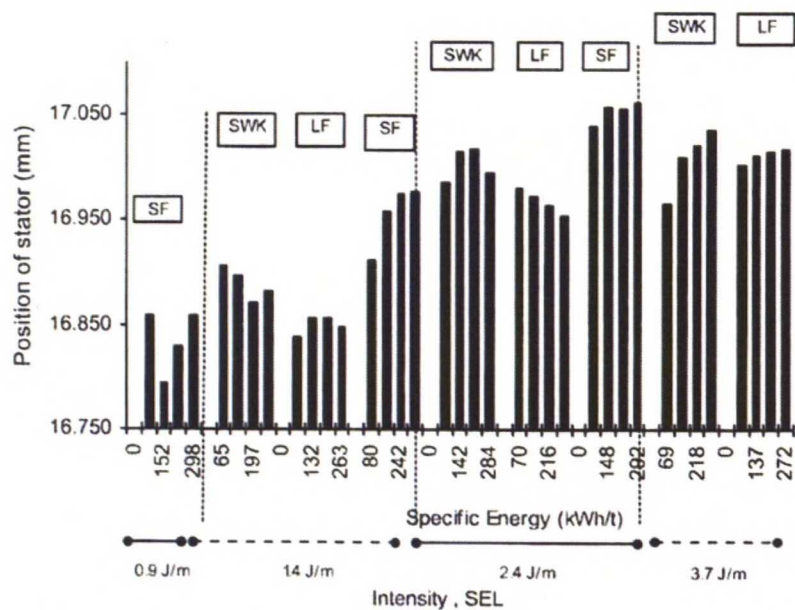
Figure 12. Changes in gap size (position of stator) for pressure-screen fractions refined under varying intensity and specific energy. Higher value of the stator position means narrower gap /9/.

4 EFFECTS OF REFINING

4.1 Introduction

If paper is made entirely from unrefined chemical pulp, it will have poor strength properties and formation because of very low fibre-bonding potential. In chemical pulp refining, fibre properties are modified by mechanical treatment in such way that fibre bonding is improved and good formation is achieved for the end product. Refining is sometimes used also to develop other paper properties such as optical properties and porosity.

4.2 Refining mechanism

One view of basic refining mechanism is shown in Figure 13. Fibres are treated with metallic bars while mixed with water to 2-6 % consistency. In the first stage of refining, fibre flocs are collected by the leading edges of the bars. Fibre floc receives a strong pressure peak at the stage when edge-to-edge contact occurs which leads to most of the water being compressed out of the floc. At this point only those fibres that remain in the floc receive the refining treatment. When edge-to-surface stage begins, the leading edges compress the fiber floc against the bar surface and most of the refining is performed. At this point the average gap width is around 100 µm which corresponds to the thickness of 2-20 fibres depending on if they are collapsed or not. The fibre floc remains compressed until the bars have crossed each other. The length of the refining impact depends on the sharpness, width and angle of the intersecting bars.

18
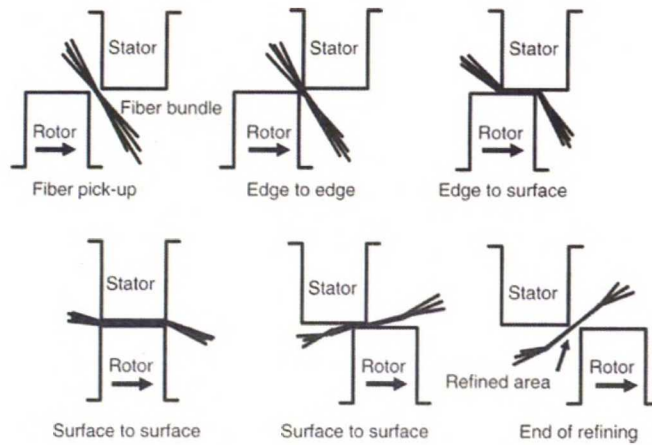
Figure 13. One view of refining mechanism of chemical pulp fibres /7/.

Page /14/ has proposed a mechanism for a single floc behavior in a refiner gap (Figure 14). Here most of the fibres are not in contact with the refiner bars, but with each other which results in friction between fibres creating shear forces. All fibres in the floc are subjected to shear forces depending on the coefficient of friction between fibre and metal or fibre and fibre.
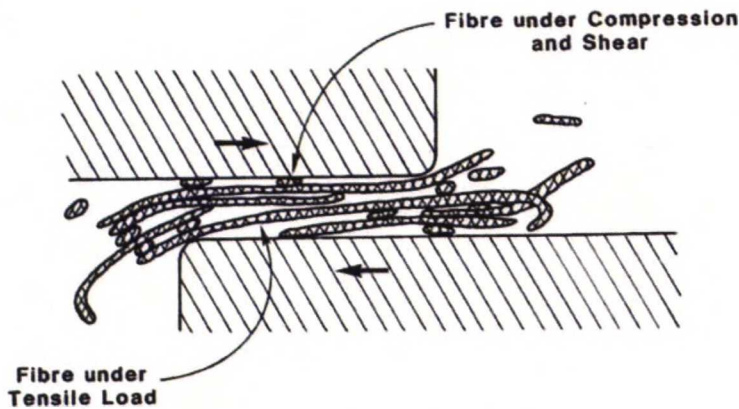
Figure 14. Impression of fibres trapped between the passing stator and rotor bars /14/.

4.3 Refining effects on fibres

4.3.1 Internal fibrillation

Fibres receive treatment during refining which forces them to compress and relax rapidly. This induces changes in the cell wall structure of the fibres. As a result

water is able to penetrate the cell wall structure and replace the internal bonds causing swelling of the celluloses and hemicelluloses. As a consequence, swelling degree, flexibility and conformability of fibres increase which leads to improved inter-fibre bonding and strength properties of paper /15, 14/.

4.3.2 External fibrillation

The most visible refining effect is the external fibrillation of fibres. This can be seen as fibrils and parts of cell wall on the surface of the fibre under microscope, as illustrated in Figure 15. External fibrillation improves the consolidation of the sheet and bonding between fibres due to the swollen celluloses and hemicelluloses that are covering the bundles of microfibrils /15/.

Figure 15. Lightly refined summerwood fibre showing sheaths and fibrils on surface. Magnification 100x /16/.

4.3.3 Production of fines

By definition, fines fraction is the part of the pulp that passes through the 200 mesh wire of a Bauer-McNett fractionator. Fines of the chemical pulp can be divided into primary and secondary fines. Primary fines are produced during pulp cooking and they consist of ray cells, parenchyma cells, bark residues and fibre fragments. The secondary fines form during the refining stage due to abrasion of fibre against each others or against refiner bars. They consist of primary wall frag-

ments, fibrils and microfibrils /17/. The primary fines content is usually below 2 %, but after heavy refining the secondary fines content can be much higher.

4.3.4 Fibre cutting and shortening

Fibre cutting and shortening are caused by the breaking of covalent bonds of the fibres. When refiner bars pass each other, the mechanical shear results to cutting and shortening of the fibres. This cutting effect is more likely to happen during early stages of the refining process when the fibres have not yet developed flexibility and increased capacity to distribute the energy /12/. Studies have also shown that lower refiner peripheral speed is likely to increase fibre shortening /1/.

4.3.5 Fibre straightening

Recent studies have indicated that the straightening of the fibres should be also considered as a main effect of chemical pulp refining. Especially in the beginning of low-intensity refining the average fibre length appears to increase because of fibre straightening /18, 2/.

5 THEORIES OF REFINING

5.1 Introduction

Many theories of the chemical pulp refining have been developed to determine the most suitable refining strategy. Jagenberg was the first scientist back in as early as 1887 to introduce such terms as "edge length per second" and "beating area" /19/. These are still used as a basis for further research. After that a number of more or less scientific theories have been developed. This part of the study will introduce most commonly accepted and some further developed theories.

The common feature for all low-consistency refining theories is that total applied refiner power is divided into net power and no-load power. No-load power should be measured by backing off refiner plates with pulp suspension flowing through the refiner. Table 2 shows the no-load power for two medium angle conical and for two double-disc refiners. Net power is the component that is affecting the fibres, and it can be calculated by deducting no-load power from total refiner power. /7/.

Table 2. No-load power of various types of refiners /7/.

Smaller refiners JC-01 and DD 20 in.			Bigger refiners JC-04 and DD 42 in.		
Speed	No load power, kW		Speed	No load power, kW	
rpm	JC-01	DD 20 in.	rpm	JC-04	DD 42 in.
1 500	150	–	750	610	–
1 200	82	130	720	550	–
1 000	50	73	600	340	390
900	40	50	514	220	250
750	27	35	500	200	230
720	24	32	400	115	120

5.2 Machine intensity based theories

5.2.1 Introduction

Machine intensity based theories take only machine parameters into account. This means that any fibre or pulp related properties are ignored.

5.2.2 Specific edge load

Brecht [20] has formulated today's concept of specific refining energy in low-consistency refining as follows:

$$SRE = \frac{(P_{tot} - P_0)}{c_F \cdot \dot{V}}$$

(1)

This can also be converted to total refining energy:

$$TRE = \frac{P_{tot}}{c_F \cdot \dot{V}},$$

(2)

where

P_{tot} is	total refining power
P_0	no-load power
c_f	pulp consistency
$\dot{V}$	volume flow.

Wultsch and Flucher [21] introduced their refining theory in 1958. They used the number of rotor and stator bars and net refining power per crossing speed to calculate bar treatment intensity. Brecht and Siewert [22] further developed this theory by demonstrating the dominant impact of the bar edge. This led to the currently used formula of specific edge load:

$$SEL = \frac{P_{tot} - P_0}{n \cdot z_r \cdot z_s \cdot \bar{l}} (J/m)$$, (3)

where

n is   rotational speed of rotor

z_r number of rotor bars

z_s number of stator bars

$\bar{l}$ average bar length.

Because the specific edge load theory does not take into account the net energy received by fibres, it has its limitations. However it is widely used because of its simplicity.

5.2.3 Modified edge load

Meltzer /23/ has recently modified the specific edge load theory by taking also the width of the bar and groove along with the average intersecting angle into account:

$$MEL = SEL \cdot \frac{1}{2 \cdot \tan \alpha} \cdot \frac{w_b + w_g}{w_b}$$, (4)

where

w_b is   width of the bar

w_g width of the groove

α bar angle.

5.2.4 Reference specific edge load

Roux /24/ has proposed a new formula for calculating specific edge load because it was seen empirically that original theory does not take into account fillings' geometrical parameter effects on fibre shortening. His version of SEL accounts for the geometrical parameters such as sum of grinding angles, sector angle and configuration of bars. Reference specific edge load is calculated:

$$C_S^0 = \frac{3(w_{b,s} + w_{g,s})(w_{b,r} + w_{g,r})}{2\pi\omega(1-k^3)} \cdot \frac{P_{net}}{r_2^2},$$
(5)

where

$w_{b,s}$ is	width of stator bar
$w_{g,s}$	width of stator groove
$w_{b,r}$	width of rotor bar
$w_{g,r}$	width of rotor groove
ω	bar peripheral speed
r_2	external rotor radius
k	ratio of internal and external rotor radius (r_1/r_2)

An expression for the normal compressive force F_n subjected onto the fibres between passing bars is formulated:

$$\frac{F_n}{\bar{n}} = \frac{C_S^0}{f\sin(\alpha + \beta + \theta)},$$
(6)

where

$\bar{n}$ is	mean number of bar crossing areas
α	stator bar angle
β	rotor bar angle
θ	sector angle.

5.2.5 Specific surface load

Specific surface load theory (SSL) was introduced by Lumiainen in 1990 /25/. He assumed that the energy is transferred to the fibre bundles also in edge-to-surface contact as well as in edge-to-edge contact. The SSL accounts for energy expenditure over bar width and is in fact an extension of the SEL theory with the value of the bar width included.

According to his concept, the refining action is described by the number, intensity and duration of the refining impacts. Specific surface load theory assumes that specific refining energy is a product of impact number and impact energy:

$$SRE = IN \cdot IE \quad \text{(kWh/t).} \qquad (7)$$

Impact energy further is a product of specific surface load and impact length which is explained in Figure 16.

$$IE = SSL \cdot IL \quad \text{(J/m).} \qquad (8)$$

$$IL = \frac{Wr + Wst}{2} \ast \frac{1}{\cos \alpha/2}$$

IL = Impact length
Wr = Width of rotor bar
Wst = Width of stator bar
α = Intersecting angle
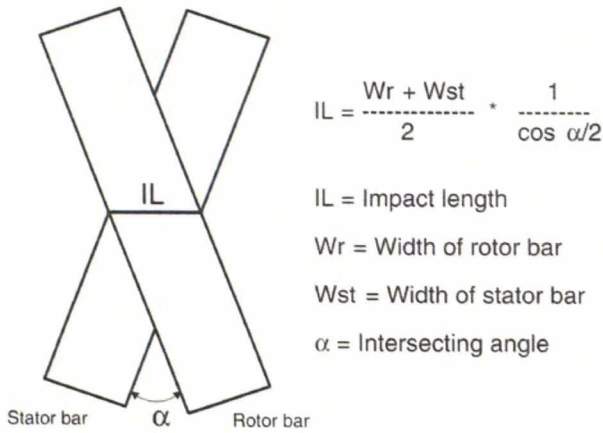
Figure 16. Definition of the impact length /7/.

Specific surface load can be now calculated:

$$SSL = \frac{P_{tot} - P_0}{n \cdot z_r \cdot z_s \cdot \bar{l} \cdot \left(\dfrac{w_r + w_s}{2 \cos\left(\dfrac{\alpha}{2} \right)} \right)} \quad \text{(N/m).} \qquad (9)$$

The specific surface load theory has partly replaced the specific edge load theory. The SSL theory seems to work well when refiner bars are so narrow that fiber

flocs cover the whole width of bar surface when receiving refining impact. On the other hand the specific edge load theory introduced earlier works better with coarse fillings when bars are wider than fibre flocs. Both of the theories have their limitations but they offer practical tools for selecting fillings and adjusting refining parameters. /7/

5.2.6 Modified specific surface load

The modified specific surface load theory (MSSL) was introduced by Musselman et al. /26/ in 1997. His theory is derived from modified specific edge load theory assuming that the stator bar width $w_{b,s}$ does not have as significant contribution on the intensity of refining as the rotor bar width $w_{b,r}$. This is due to the fact that the rotor was assumed to account for the transportation of fibres onto the stator bars. MSSL is calculated:

$$MSSL = \frac{P_{tot} - P_0}{n \cdot z_r \cdot z_s \cdot \bar{l} \left[\dfrac{w_{b,r}}{\cos\left(\dfrac{\alpha}{2}\right)} \right]} \text{ (J/m}^2\text{)}. \tag{10}$$

5.3 Fibre based intensities

5.3.1 Introduction

In addition to the machine parameters, fibre based intensities include also more or less fibre and pulp properties. This leads to a more accurate but also more complex theories of the refining phenomenon.

5.3.2 Floc hypothesis

In 1990, Hietanen and Ebeling /27/ proposed a new theory for the mechanics of chemical pulp refining. The role of fibre flocs in refining has been under discussion since 1920's and after that various authors have dealt with this phenomenon.

Floc hypothesis theory is based on the assumption that in low consistency refining (2-6 %), fibres are refined as flocs instead of independently receiving treatment. Flocs are continuously formed and broken up under the shear forces in the refining zone and grooves. Excessive refiner energy is consumed in maintaining turbulent conditions when flocs are transported through the refining zones without undergoing any refining treatment.

The thickness of individual flocs in low consistency refining is normally 1-5 mm. They are relatively large compared to the size of the refiner gap, which is usually 50-150 μm. For this obvious reason the probability that flocs will be driven into the gap is low resulting in much larger volume of pulp flow being driven through rotor and stator grooves than through the gap. This gives a heterogeneous refining result where some fibres have lost their shape completely because of the harsh treatment while some fibres do not show any structural changes at all.

Floc hypothesis theory introduces a modern approach for increasing refining efficiency and homogeneity. Designing the refiner zone so that all or most of the fibres entering it undergo treatment would enable more homogeneous refining result. The volume of the refining zone should also be minimized to enable the refining work to be concentrated on a small fluid volume. This gives the fibres a possibility to receive a more energy efficient and homogeneous treatment.

Laboratory scale tests have been made with a small disc refiner that was built based on the concept of floc hypothesis theory, and the results are promising. However at this time no production scale refiner has been developed based on this theory.

5.3.3 Frequency and intensity

Lewis and Danforth /28/ attempted to describe the refining process with two independent expressions. The number of impacts describes the amount of treatment received by fibres and the severity of impacts described the type of treatment.

Also the pulp properties were included in the calculations through pulp consistency. Figure 17 shows an illustration of this theory.
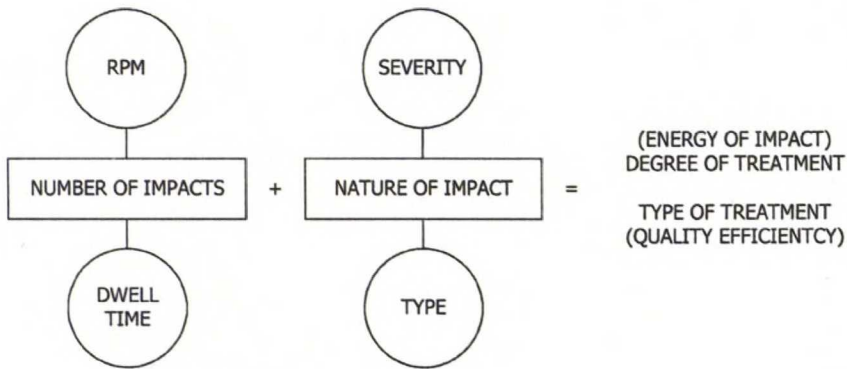
Figure 17. Effect of number and nature of impacts on type and degree of refining treatment /28/.

Danforth later developed this theory into two equations. The equation for severity of impacts is:

$$S = \frac{(P_{tot} - P_0) \cdot A_t}{D \cdot (RPM) \cdot L_r \cdot L_s \cdot c} \cdot K_2 \quad , \tag{11}$$

and for number of impacts:

$$N = \frac{L_r \cdot L_s \cdot (RPM) \cdot c}{X \cdot R} \cdot K_1 \quad , \tag{12}$$

where

A_t is	total area of refining zone
D	effective diameter
RPM	rotor revolutions per minute
L_r	total length of rotor edges
L_s	total length of stator edges
c	stock consistency

X	average bar contact length
R	throughput rate
K_1, K_2	constants.

Most of the factors affecting refining result are included in this theory. However because its complexity and constants that are not easily available, it is not so commonly used.

5.3.4 C-factor

Kerekes /29/ introduced a more comprehensive approach on refining effects in 1990. Using the same approach as Lewis and Danforth, he derived net refining energy as a product of number and intensity of the impacts:

$$E = N \cdot I \tag{13}$$

Figure 18 shows the different effects of refining intensity and frequency on the refining result with similar energy consumption.
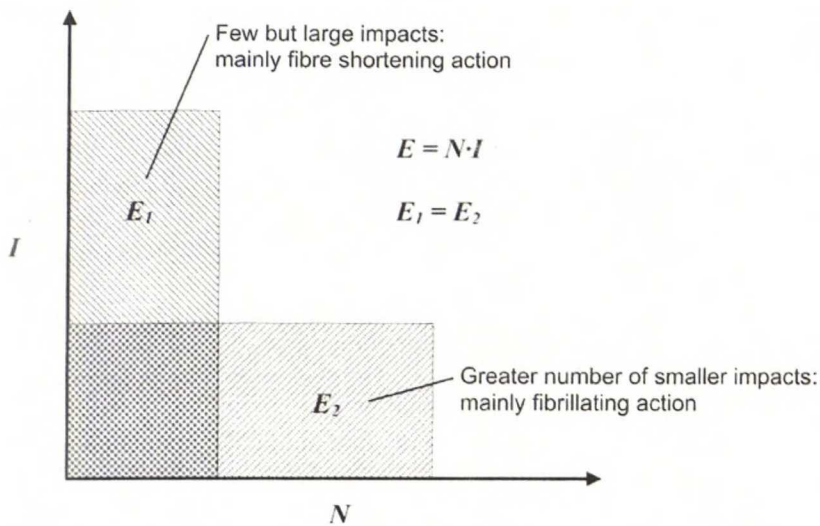
Figure 18. The two combinations of refining intensity and frequency effects on the refining result /29/.

C-factor represents the capacity of a refiner to inflict impacts on pulp fibres. Kerekes has approached the refining process also from the pulp properties point of view instead of concentrating only on machine parameters and process variables. The C- factor connects the net power input P_{net} and pulp mass flow rate F, to the average number N and intensity of impacts I by the following equations /7/:

$$N = \frac{C - factor}{F} \tag{14}$$

$$I = \frac{P_{net}}{C - factor}. \tag{15}$$

The C-factor is a function of refiner filling geometry, rotation speed, pulp consistency, fiber length and coarseness.

For a disc refiner in simplified conditions where the gap size is small and the bar pattern is similar on both rotor and stator, the C-factor is given by the following equation:

$$C = 8 \cdot \pi^2 \cdot G \cdot D \cdot \rho \cdot C_F \cdot l \cdot n^3 \cdot \omega \cdot (1 + 2 \tan \phi) \cdot \\ (R_2^3 - R_1^3)/ 3 \cdot w \cdot (l + D) \tag{16}$$

and for a conical refiner in simplified conditions:

$$C = 8 \cdot \pi^2 \cdot G \cdot D \cdot \rho \cdot C_F \cdot l \cdot n^3 \cdot \omega \cdot (1 + 2 \tan \phi) \cdot \\ [R_1^2 \cdot L + L^2 \cdot R_1 \sin \theta + (L^3/3) \sin^2 \theta]/ w \cdot (l + D) \tag{17}$$

where

G is	width of grooves
D	depth of grooves
ρ	density of water
C_F	pulp consistency

l	length of fiber
n	number of bars per unit arc length of rotor/stator
ω	rotational velocity of refiner
ϕ	bar angle on rotor/stator
R_1	inner radius of disc refiner plate
R_2	outer radius of disc refiner plate
w	coarseness of fibre
L	length of refining zone
θ	angle of conical refiner.

C-factor analysis is probably the most comprehensive refining theory developed so far. It also builds on other widely used and well known theories such as specific edge load and specific surface load. However for example fillings wear can have an effect on C-factor. Because these factors can be difficult to determine and calculations are sometimes very complex, this theory is not widely used among papermakers /7/.

5.4 Conclusions about refining theories

If full understanding and control is targeted, theories including fibre and pulp properties seem logical. There are some results which imply that the refining effect on fibres is described well by the C-factor theory. Similar unpublished results have been received in studies conducted in Finland /30/. Theories based simply on machine parameters and data have practical use. As there does not seem to be clear advantages in any specific one, for papermakers it has been reasonable to use the simplest one: The specific edge load theory (SEL).

6 REFINING ENERGY AND FORCES

6.1 Force acting on pulp mass

Shear stress acting on pulp mass is dependent on specific edge load, sliding distance, partial bar and partial fibre coverage by equation:

$$\sigma_F = \frac{SEL}{b \cdot z \cdot s}, \tag{18}$$

where

SEL is	specific edge load
b	length over bar width covered
z	fractional bar coverage
s	sliding distance.

6.2 Forces acting on individual fibres

Quantifying forces acting on individual fibres can be difficult because of the large distribution of forces within fibre networks. Kerekes and Senger /31/ have estimated the average normal force acting on a fibre by the equation:

$$f_N = \frac{\sqrt{\pi} \cdot d_0 \cdot l^{\frac{3}{2}} \cdot C_s \cdot \sqrt{kG}}{4 \cdot a \cdot T} \cdot \left(\frac{SEL}{\pi \cdot S \cdot b \cdot z} \right)^{0,7}, \tag{19}$$

where

d_0 is	uncompressed fibre diameter
l	fibre length
C_s	consistency of the floc before compression
k	fractional proportion of the groove from which fibres are captured
G	groove width
T	gap size
SEL	specific edge load

S	sliding distance
z	fractional distance along unit bar length covered with fibre
a, b	constants.

Values of some of the constants in this equation are not known at the present time /32/. One target of this thesis is to be able to measure fractional distance along unit bar length covered with fibre z, and possibly consistency of the floc before compression C_s.

Figure 19 shows a simple example of the effect of the bar coverage on forces acting on fibres. With smaller bar coverage, the normal force on a single fibre is increasing linearly due to the distribution of the force on a smaller area.

$$f_n = \frac{F_n}{2} \qquad\qquad f_n = \frac{F_n}{10}$$
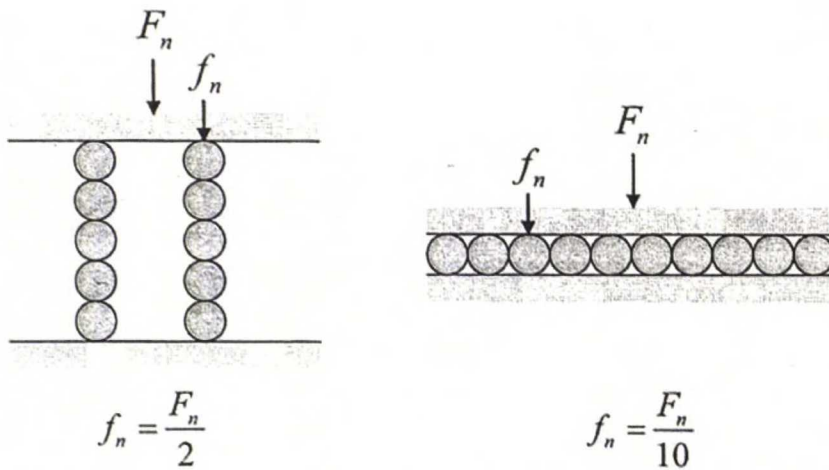
Figure 19. Simplified example of how smaller fractional bar coverage gives a larger force on fibres f_n than do more evenly distributed fibres for the same bar normal force F_n /32/.

The shear force on a fibre can be calculated from the normal force by an effective coefficient of friction

$$f_S = \mu_E \cdot f_N.$$

Martinez and Kerekes /33/ measured a typical shear force distribution along the width of the bar surface of a single-bar laboratory refiner they constructed. Figure

20 shows that the force peaks to a maximum at a time of 0.35 s which corresponded to a distance of around 3-5 mm (total bar width was 10 mm) from the leading edge. Several studies conducted afterwards confirm this type of distribution also for normal force /34, 35, 36/ except for the magnitude which is usually 10 times higher than with shear force.
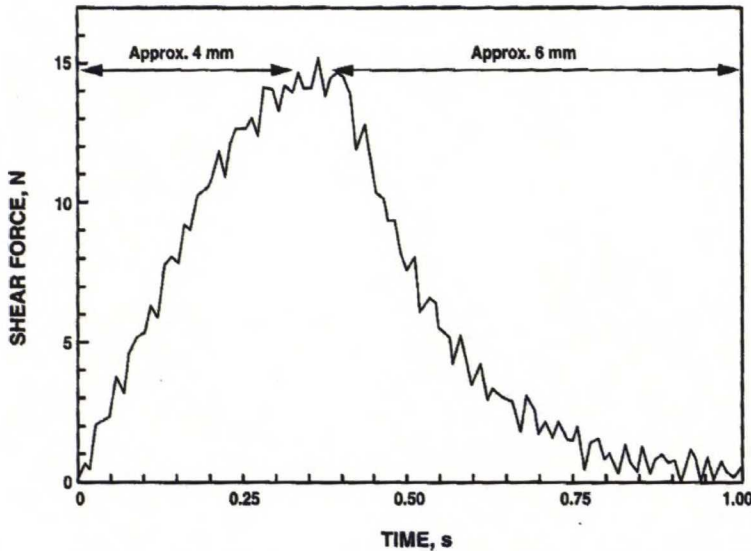
Figure 20. A typical shear force distribution along the width of the bar surface /33/.

6.3 Energy efficiency in refining

Refining effects are produced by breaking of molecular bonds caused by forces which create strains in fibres. According to Kerekes, force balances link bar action to fibre deformation, which permits comparison between energy expended and energy transferred. This theoretical efficiency is very low varying according to different studies from 0.2 % to 15 %. Bar energy is also transferred to fibres as external fibrillation and surface fines production as they depend on both force and sliding distance. However the true energy efficiency is not known because of the process constrains set by quality considerations. /32/

As mentioned earlier, refining can be divided into three phases which are:

- Edge-to-edge

- Edge-to-surface
- Surface-to surface.

All of these phases consume energy and the effective part of it is transferred to the fibres. The no-load power remains as constant during the refining impact. Total refining energy is split between the phases as shown in Figure 21.
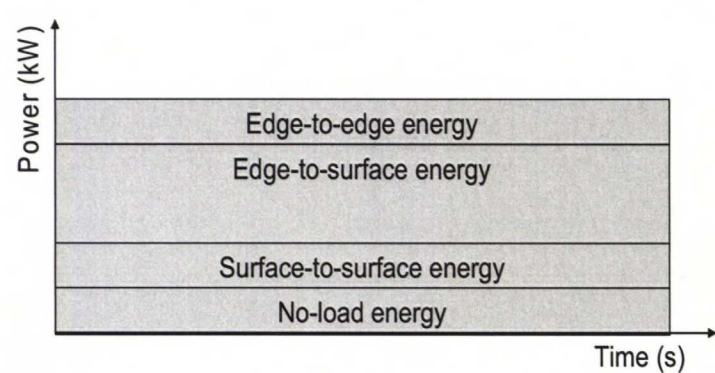
Figure 21. Total refining energy split as presented by Lumiainen /37/.

When the leading edges approach each others the power quickly reaches its maximum value. After this phase it decreases to the no-load energy level as illustrated in Figure 22. However since all phases occur simultaneously, the total power consumption remains at a constant level.
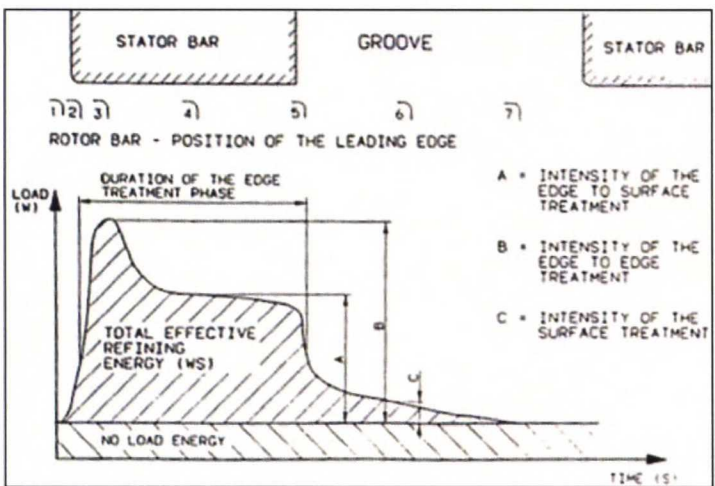
Figure 22. Intensity and duration of the refining impact.

7 CONCLUSIONS OF THE LITERATURE REVIEW

There are many different theories developed concerning low-consistency refining and its effect on pulp and fibres. Despite the fact that it is one of the most researched areas of papermaking, many unknown issues still remain. These include parameters such as bar coverage and pulp consistency in the refining gap. Many of the studies conducted in the earlier days concentrate mostly on the machine parameters rather than pulp or fibre related parameters. This has lead to the use of the simplest theories, such as specific edge load (SEL) theory when controlling the refining process. Understanding of the forces acting on pulp and even individual fibres during refining is still very much an unknown issue. There are some studies that have concentrated on measurement of normal and shear forces on fibres during refining in the past decades, but more research in this area is definitely required.

8 EXPERIMENTAL

8.1 Target

Target of the thesis work was to construct a Single Bar Refiner station in order to enable measurement of fractional bar coverage and pulp consistency in the gap between rotor and stator bars by image analysis. Improved knowledge of the low consistency refining phenomenon is expected to provide potential for energy savings in low-consistency refining of chemical pulp and possibly also in thermomechanical pulp refining (TMP). Also improving quality control by for example introducing novel refiner constructions and tailor-made refining for different end uses could be some of the future innovations.

The experimental section of this thesis describes the designing and construction process of the Single Bar Refiner station in detail. There were also some preliminary trials that were conducted with the refiner, which included the imaging system testing. Results from those trials are also included in this section. The SBR station was placed to the machine hall of TKK Forest Product Department and will be mainly operated by Paper and Printing technology group.

8.2 Background

Starting point of this thesis was linked to an earlier project where first version of the Single Bar Refiner, later referred as SBR, was constructed by modifying the chamber of a pump. The rotor shaft of the pump was fitted with a cylinder equipped with two bars to create a refining effect on the fibres passing between the stator and rotor bars (Figure 23).
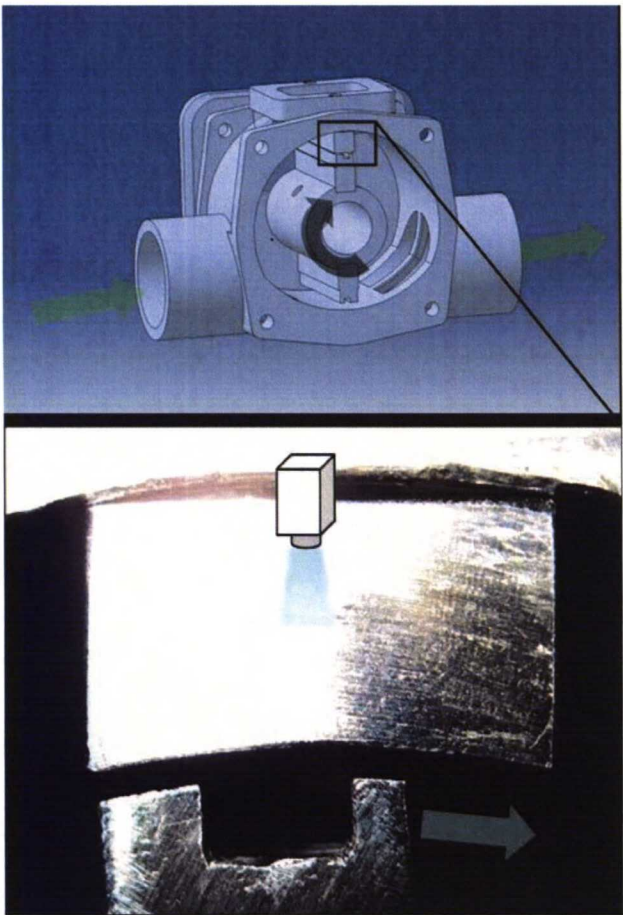
Figure 23. The refining gap on the first version of the Single Bar Refiner unit /4/.

The stator bar was installed on the upper side inside the chamber. In the first version of the refiner, the rotor bar was grooved and the stator bar was flat. The imaging could be conducted from the above through an acrylic window which was also part of the stator bar, or from the front side through an acrylic plate (Figure 24).
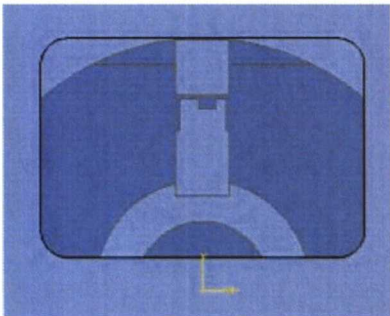
Figure 24. The front window of the refiner unit /4/.

The first version was tested only shortly due to the ENGINE project closure, but the results were promising. Some good images and video material was shot and also a technique for image analysis was developed /4/. After the construction of the refiner some modifications were suggested to create more realistic refining conditions in the gap between the bars. Because of the stator design (no groove), the fibre capture was not realistic enough because the fibres were captured in the refining zone from a much larger volume than in real situation. Grooving the stator bar would create a finite volume for the pulp suspension and was expected to have an effect on the fibre behavior in the gap. Also the size of the refining gap between stator and rotor bars was unrealistically large.

8.3 Modification of the stator bar

8.3.1 Introduction

One of the main targets of the SBR construction was to design a stator with two bars with a groove between them instead of only one wide bar, as was the case in the first version. Second important modification was to decrease the gap between stator and rotor bars to a more realistic value of 150 μm - 300 μm from the original gap size which was estimated to be ~500 μm.

8.3.2 Grooving the original stator bar

The modification of the SBR stator bar was started by designing a groove on the stator bar used in the original setup. The groove dimensions were similar to the ones used in the rotor bar (Figure 25).
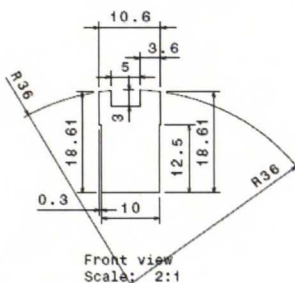
Figure 25. Dimensions of the rotor bar /4/.

The stator bar consisted of a stainless steel and acrylic parts that were connected to each others. The acrylic part was installed outside the refiner casing between a metal frame and the stainless steel part. Two M6 bolts were used to keep the parts together and attached to the casing. The groove was machined on both parts 5 mm wide from the center to a depth of 3 mm. Figure 26 and Figure 27 describe the structure of the grooved acrylic and stainless steel parts.
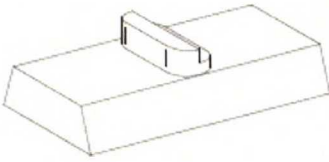
Figure 26. Structure of the acrylic part of the SBR stator bar.
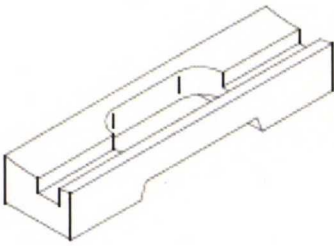
Figure 27. Structure of the stainless steel part of the SBR stator bar.

With this modification the designed structure could be tested with the original gap size to see the behavior of the refiner. The results of these trial runs are discussed later.

8.3.3 Reducing the gap size between refiner bars

Introduction

Two different methods were considered to reduce the gap between the rotor and stator bars to the wanted level of 150 μm – 300 μm. First method under discussion was to use some type of shims at certain points of the stator structure to adjust the gap. Another option was to design new acrylic and stainless steel parts for each gap size desired. Because of the difficult design of the stator bar, using new parts

was considered as more useful approach than adjusting the gap size with shims. The starting point was to design two sets of parts, first set for the gap size of 150 μm and the second one for the gap size of 300 μm.

Measuring the original gap

First problem was to measure the gap size from the original refiner structure to be able to define exact dimensions for the new parts. This was accomplished by first taking a photograph from the side of the refiner unit at the point where the rotor and stator bars are parallel to each other (Figure 28).
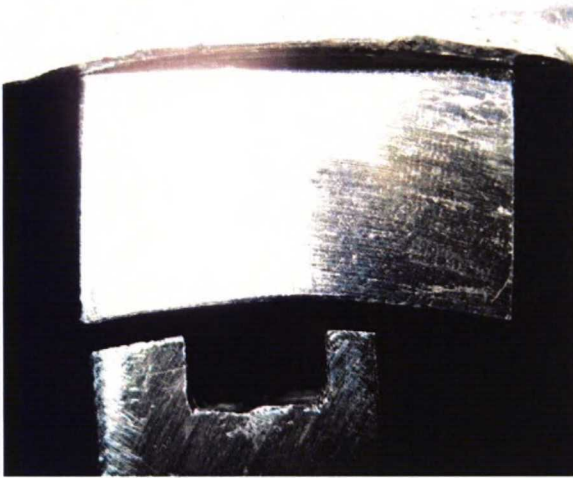
Figure 28. Picture of the rotor bar and the original stator bar (without groove).

From this photograph it was possible to determine the relation of the gap clearance to a known dimension (in this case bar height) and then calculate the gap size:

$$g = \frac{P_g}{P_b} \cdot b \quad , \tag{20}$$

where

P_g is   gap size [pixels]

P_b bar height [pixels]

b bar height [mm].

The measured bar height was 9,1 mm / 740 pixels and gap size 83 pixels. We can now calculate the gap size of the original setup using equation 20:

$$g = \frac{P_g}{P_b} \cdot b = \frac{83\,pix}{740\,pix} \cdot 9,1mm = 1,0mm.$$

Designing the new stator bars

The dimensions for the new acrylic and stainless steel parts could now be calculated from the original gap size. For example bar height for new stainless steel part:

$$b_x = b + (1,0mm - g_x),$$
(21)

where

g_x is   desired gap size.

For a desired gap size of 300 μm we get a bar height of:

$$b_{300} = 9,1mm + (1,0mm - 0,3mm) = 9,8mm.$$

By measuring the dimensions of the original acrylic and stainless steel parts and using this information, drawings for all new stator components could be designed using Solid Edge CAD software. Drawings with all the dimensions are included as appendices 1-4.

Fitting the new stator bars

When the new stator bar parts designed for the gap size of 150 μm were installed, the rotor was not able to rotate because the bar seemed to be too high. With the parts designed for the gap size of 300 μm, the rotor could barely slide past the stator bar. This problem occurred probably because of the errors in measuring the

original gap size. Because the measurement was made only from one side of the stator – rotor contact, irregularities along the length of the stator bar were not visible and therefore could not be taken into consideration.

The solution to this problem was to assume that the new stator parts were 300 μm too high. This in fact was the case because the gap size was actually 0 when a gap size of 300 μm was wanted. This is due to the fact that the rotor was touching the stator while still able to slide past it. This lead to a conclusion that the original gap size was actually 700 μm instead of the 1000 μm calculated earlier. As a result, a 300 μm chip was taken off from both of the stainless steel parts and 300 μm shims were used under the acrylic parts to keep the refiner casing sealed.

8.4 Pulp flow system design

To enable even pulp flow through the refiner, a flow system with recirculation was designed (Figure 29). A steel reinforced clear PVC hose with an inner diameter of 32 mm was chosen for fluid transportation because of its flexibility, durability and relatively low price. Manually operated globe valves were chosen for process points where control of the flow was considered necessary. These points are:

- After the pulp disintegrator to drain the suspension to the storage tank
- After the storage tank to open/close access to the flow system
- Two points after the pump to control flow direction and speed to the refiner and back to the storage tank (recirculation).
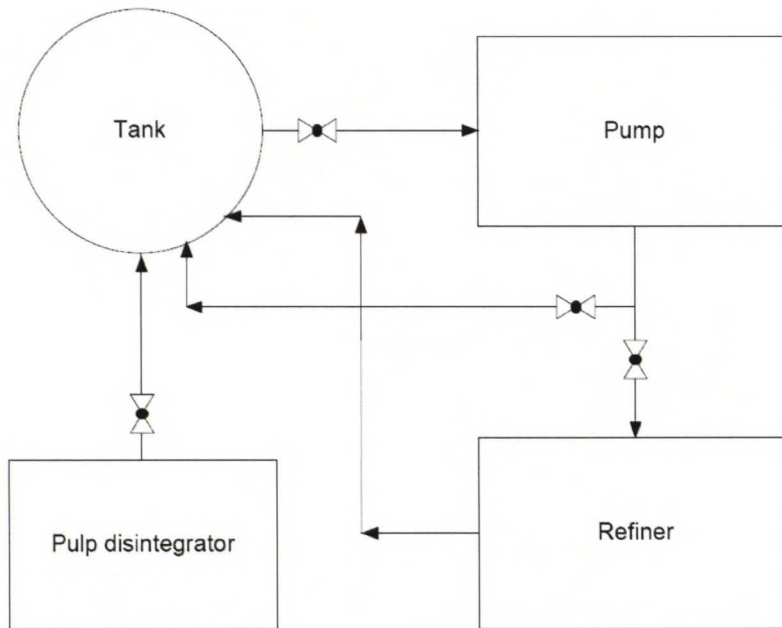
Figure 29. Pulp flow chart and position of the globe valves.

8.5 Layout and components

8.5.1 Layout design

The refining station includes following components:

- Pulp disintegrator
- Tank
- Pump
- Refiner unit
- Imaging system

The imaging system includes a camera, laser unit equipped with fiber optics for illumination, control unit and a laptop computer. These were mounted on two separate tables to ensure dry operation conditions for the computer and control unit.

Figure 30 describes the layout design and location of the components. The most challenging part of the layout design was the limited space allocated for the refiner station. The dimensions were limited by three walls and a large electric motor used for other applications in the machine hall. The refiner station was installed in the base floor of machine hall (PUU 1) next to the large pulp disintegrator.
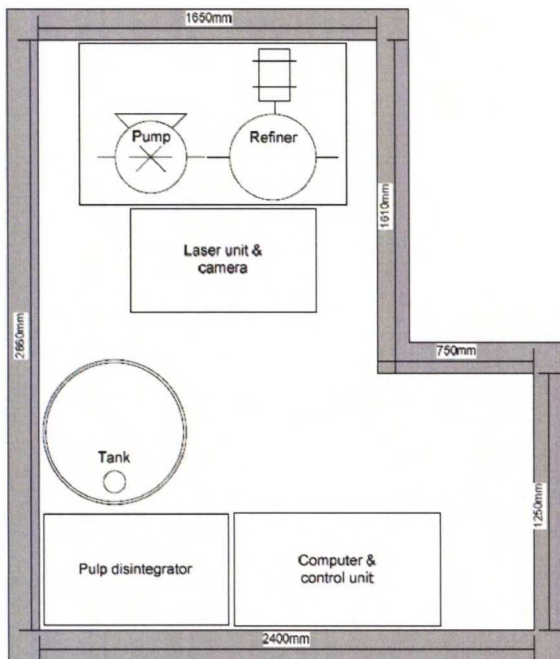
Figure 30. Single Bar Refiner Station dimensions, layout and components.

8.5.2 Components of the refiner station

Pulp disintegrator

Before operating the Single Bar Refiner, pulp has to be disintegrated. A laboratory scale vertical pulp disintegrator was installed for this purpose (Figure 31). With a capacity of 43 dm³ it was suitable for this application. It is equipped with a 3 kW electric motor which runs at 2800 rpm when empty. The disintegrated pulp suspension can be drained after operation via a globe valve located in the bottom.

Figure 31. A laboratory scale pulp disintegrator used for slushing the dry pulp.

Storage tank

The amount of pulp in the flow system was calculated in order to estimate the minimum size of the pulp storage tank needed. This was then multiplied by three to ensure good flow conditions:

$$V_{min} = 3l\pi r^2,$$ (22)

where

l is   total length of the flow circulation [m]

r radius of the hose [m].

In this case the total length of the circulation is 10 m and the radius of the hose is 16 mm so using equation 22 the minimum volume can be calculated:

$$V_{min} = 3l\pi r^2 = 3 \cdot 10m \cdot \pi \cdot (0,016m)^2 = 0,024m^3 = 24dm^3.$$

A steel tank with a volume of 142 dm³ was installed to store the pulp suspension during operation of the refiner (Figure 32). There were also some other second-

hand storage tanks available in the machine hall but this one was the best option because of its compact size and high capacity. In this perspective the capacity of the tank is high enough for this application and also for possible future modifications to the pulp flow system. It is also practical to conduct consecutive tests with different pulp consistencies because of the extra capacity for dilution water.

Figure 32. The tank used for storing the pulp suspension.

Pump

To create flow conditions for the refiner unit, a gear pump (Figure 33) was installed after the storage tank. It had been used earlier for transportation of pulp suspensions in the machine hall and was available, which made it optimal for this use. The pump is also powerful enough to mix the pulp suspension in the storage tank when recirculation valve is open which makes an additional mixer unnecessary.

Figure 33. The pump used in the pulp flow system.

Refiner unit

The refiner unit was constructed by modifying the chamber of a pump. This was done by replacing the pump rotor with a part that acts as a refiner rotor. The rotor has two metal bars located symmetrically around the rotor cylinder. This creates two contacts of the stator and rotor bar per one revolution of the drive shaft. Both bars were grooved with a width of 5 mm and a depth of 3 mm which corresponds to the dimensions of the grooves used in the Voith LR 40 laboratory refiner at TKK and were therefore chosen here. A metal bar fitted with an acrylic imaging window was attached on top of the pump casing which enabled image capture of the events that take place in the refining gap. The power of the refiner motor can be adjusted within a scale of 0,15 kW – 0,75 kW.
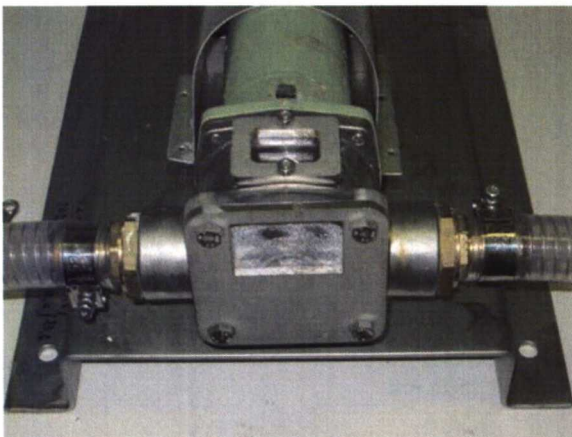
Figure 34. The Single Bar Refiner unit. Flow direction is from left to right.

As mentioned earlier the refiner unit and rotor were designed and constructed as a part of ENGINE –project discussed in the introduction of the experimental section. Only the design and modifications on the stator bar and the motor on the refiner were changed as part of this thesis.

The imaging is conducted from above the refiner through the acrylic part of stator bar. The position of the bars and illustrative description of the imaging is shown in Figure 35.
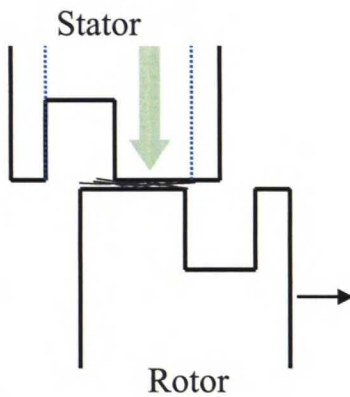
Figure 35. An illustrative description of the imaging process.

8.6 Imaging system

8.6.1 Introduction

The imaging system for capturing images inside the gap between the rotor and stator bars was designed to enable image analysis of the fibre behavior during the refining phenomenon. Some similar methods to capture fibres during refining using photography has been used by various researchers in the past decades /38, 39, 40/. However these studies have concentrated mostly on thermomechanical pulp refining, so imaging method for low-consistency refining of chemical pulp with this type of laser imaging system has not been published. The main target of the

image analysis was to study the possibility to measure pulp consistency and fractional bar coverage in the gap between the stator and rotor bars.

All components of the imaging system were supplied by Cavitar Oy, a company which is specialized in projects that require laser illuminated imaging. The laser illumination was needed to capture sharp high resolution images from fibres and fibre flocs captured between the bars during refining. The system with its components and connections are described in Figure 36.
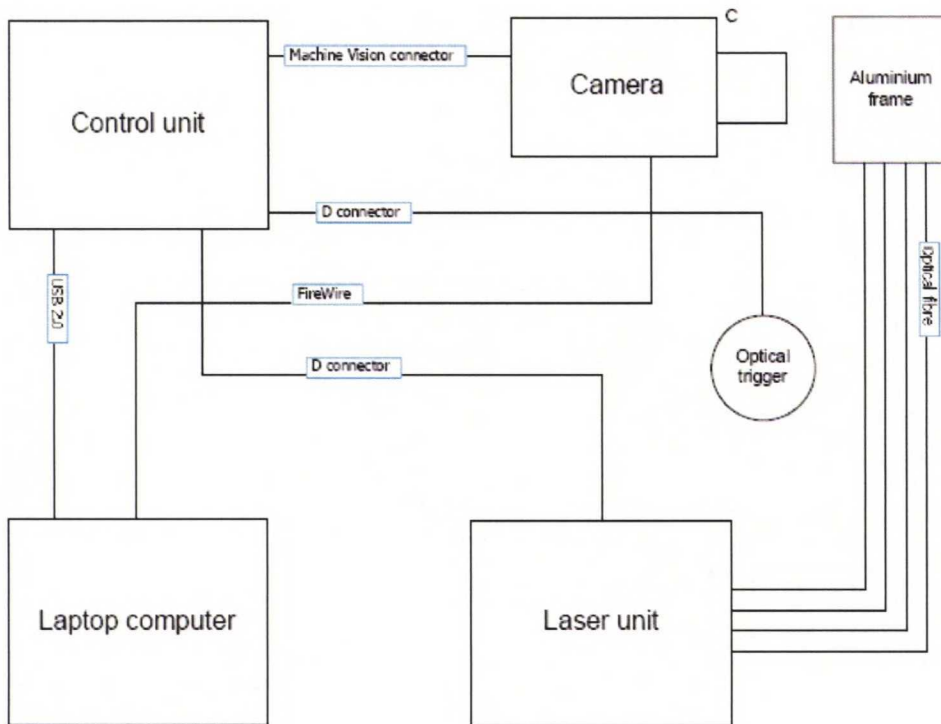
Figure 36. The imaging system components and connections.

8.6.2 Control unit

The control unit (Figure 37) is used by the computer software to operate the imaging equipment. It has independently programmable outputs for the laser unit and the camera. The duration of a single pulse within the output pulse pattern can be adjusted to a value between 42 ns – 10 µs. The unit has a 9-pin D connector and a BNC connector for external synchronization purposes and a Remote Interlock

connector which can be used to stop the operation of the imaging system for safety reasons (not used in this setup). The control unit has a manual adjustment for the laser power and a key operated master control for power.

Figure 37. The imaging system control unit.

8.6.3 Camera

A PixeLINK™ PL-A741 machine vision camera with a telecentric 55 mm lens was attached to a table with a mounting arm (Figure 38). It is a 1,3 megapixel monochrome camera which is connected to the computer with a high speed Fire-Wire interface. Because the laptop computer could not provide power to the camera via the FireWire bus, an external 12 V DC power supply was needed. The camera is connected to the control unit with a 6-pin Machine Vision connector. Some basic features of the camera are described in Table 3.

Figure 38. The installed camera and lens with mounting arm.

Table 3. Basic features of the PL-A741 machine vision camera /41/.

Feature	Supported	Unit	Type	One-Push Auto	Read Out	On/Off	Auto	Manual	Min Value	Max Value
Brightness	Yes	%	Absolute	No	Yes	No	No	Yes	0	100
Shutter	Yes	s	Absolute	No	Yes	No	No	Yes	0.00004	1
Gain	Yes	dB	Relative	No	Yes	No	No	Yes	0	
Temperature	Yes	°C	Absolute	No	Yes	No	No	No		
Trigger	Yes			See trigger mode descriptions (on page 33)						

8.6.4 Laser unit and fibre optics

The laser unit (Figure 39) is providing laser pulses for illuminating the area where images are captured. It can provide 500 watts of light power as a single pulse in a wavelength of 690 nm which makes it a class 4 laser product. This means that proper safety precautions must be taken when operating the unit. The laser unit is resistant to splash water so it could be safely installed near the pulp flow system. It is connected to the control unit with a 9-pin D connector.

Figure 39. The imaging system laser unit.

The pulse of light is transferred from the laser unit via a fibre optic cable through an aluminum frame. A bundle of optical fibres divide the light inside the frame to provide uniform illumination through the acrylic part inside the gap between rotor and stator bars. Figure 40 shows the position of the aluminum frame and optical fibres on top of the refiner unit. The images can be taken from the opening located in the middle of the frame.
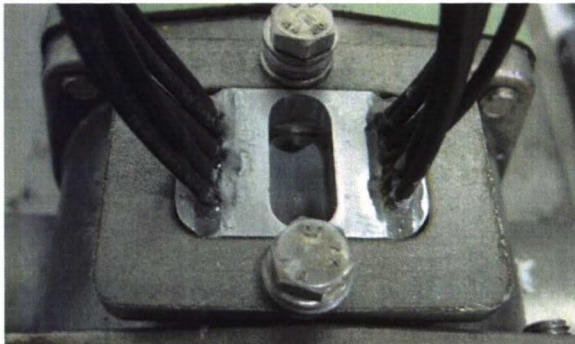
Figure 40. The aluminium frame with bundle of optical fibres installed on top of the refiner unit.

8.6.5 Optical trigger

In order to synchronize the camera to capture images from the same position for each revolution of the refiner, an optical trigger was installed on the refiner unit (Figure 41). The trigger consists of a cable and a light beam sensor which sends a 5 V electric signal when the beam is interrupted. A metal bar was attached to the coupling between the refiner unit and its motor in a position where the stator and rotor bars were aligned. The purpose of the bar was to interrupt the light beam once per each revolution of the refiner rotor to trig the signal for the control unit. The final adjusting of the exact moment of image capture was made in the control software by creating a delay signal for the camera and laser outputs.
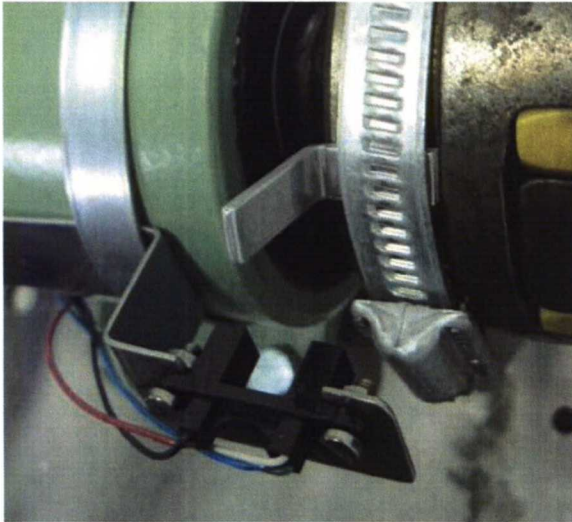
Figure 41. Metal bar crossing the light beam of the optical trigger.

8.6.6 Computer and software

The imaging system is controlled with a laptop computer using CAVILUX control software. The software can be operated either in normal or high speed mode which is convenient if using high speed camera. Because we are operating the PL-A741 camera for capturing still images, normal mode is used. The software enables programming of different pulse patterns for the camera and laser unit to adjust synchronization with the process.

Image capture software from Pixelink was used in recording the images on the computer. It was also possible to adjust all the camera parameters and settings such as exposure time, brightness, image size and frame rate with this software. Figure 42 shows a screen capture of the control software in the parameter set mode presenting the pulse patterns used in preliminary trials, and the image capture software settings. All the program settings are presented in appendix 5.
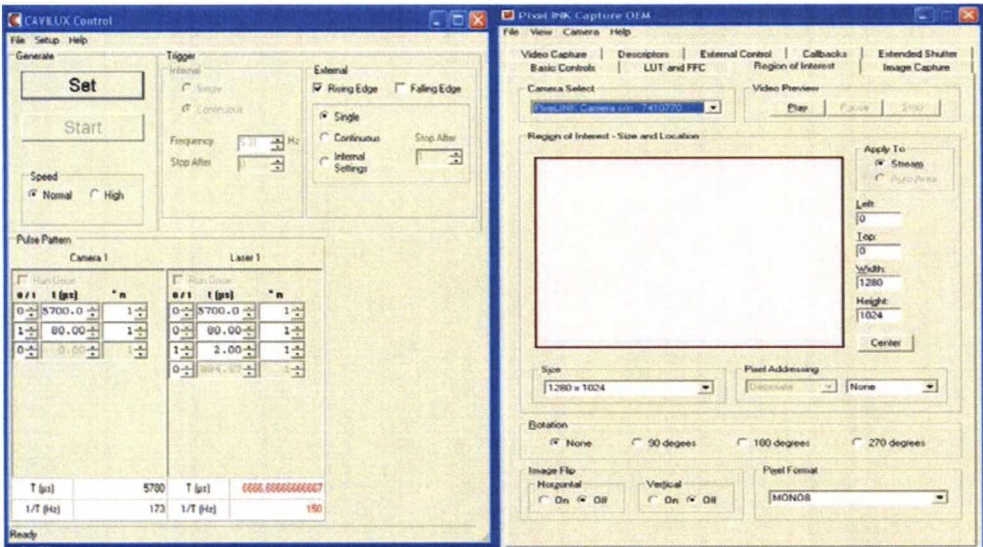
Figure 42. Screen captures from the CAVILUX control and PixeLINK image capture software.

8.6.7 Safety equipment and accessories

Safety glasses

Safety glasses were purchased to prevent eye injury during the operation of the laser illuminated imaging system. The model "LG7 Teal Lens" glasses (Figure 43) provide good protection for the 690 nm laser light while still enabling 35 % of the visible light to pass through the lenses and were therefore chosen.

Figure 43. The LG7 Teal Lens protective glasses from Thorlabs Inc.

Additional lens and illumination optics

If there is a need to capture images from the front side window of the refiner, an additional lens is available to generate an appropriate image size. In this type of imaging system setup the laser illumination is provided from the front side by using an adjustable optical cable with the laser unit instead of the aluminum frame. In this thesis all the images were captured from above the refiner.

8.7 Process description

8.7.1 Introduction

The process of the SBR station operation can be divided to three stages described in Figure 44. Before the actual operation of the refiner, the pulp suspension has to be properly disintegrated and diluted to a desired consistency. The operation of the flow system includes the refiner, pump and globe valves. The imaging can be started when the flow system is set up. This chapter includes a more detailed description of each stage.
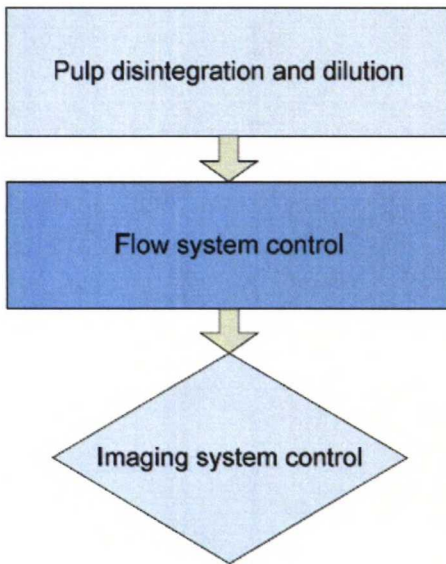
Figure 44. The process of the Single Bar Refiner station operation.

8.7.2 Pulp disintegration and dilution

Before starting the refiner, dry pulp sheets must be mixed with water and slushed in the pulp disintegrator. Optionally never-dried pulp can be used. The rotor inside the disintegrator creates strong shear forces which result in a flowing pulp suspension. The consistency of the suspension in the laboratory pulper should be < 5 %. Any higher consistency would make the draining of the suspension after the pulping difficult and the durability of the power transmission belt would also suffer. The disintegration time should be 5 minutes or more in order to generate a homogenous pulp suspension. The consistency of the pulp suspension after disintegration is:

$$c_p = \frac{m_p}{(m_p + m_w)}, \qquad (23)$$

where

m_p is   amount of dry pulp [kg]

m_w amount of water [kg].

After the disintegration pulp is drained from the globe valve to the storage tank where it is diluted with water to a desired operation consistency. The amount of dilution water required depends on the consistency after pulp disintegration, amount of the pulp suspension and the desired refining consistency:

$$m_{w,d} = \frac{c_p \cdot (m_p + m_w)}{c} - (m_p + m_w), \tag{24}$$

where

c_p is   consistency after pulp disintegration [%]

c desired refining consistency [%].

8.7.3 Flow system control

The pulp flow system is controlled by the pump and two manually operated globe valves (Figure 45). The function of the valves is to control the pulp flow through the refiner and back to the storage tank. The valve to the storage tank is normally fully opened when operating the refiner in order to create high enough flow rate to enable mixing of the pulp suspension in the tank. The valve to the refiner is then adjusted to control the flow through the refiner. Both the pump and the refiner have protective switches on the wall of the SBR station. The flow system is operated by switching the power to the pump and refiner on and then adjusting the recirculation flow and flow through the refiner with the globe valves.

Figure 45. The globe valves used for controlling the pulp flow.

8.7.4 Imaging system control

The imaging system is set up as described in Figure 36. When all the cables are connected and the control unit and the computer power is on, the camera lens has to be focused on the area where stator and rotor bar slide past each others. This is done by first adjusting the camera to a distance of ~15 cm from the targeted area and then fine tuning the focus from the lens. After the focusing is complete, imaging system is ready to use.

Synchronizing the camera to capture images at exactly the desired moment is done by first adjusting the optical trigger roughly to the correct position of the refiner bars. The exact position of the bars during image capture is then fine tuned by creating a suitable delay signal on the image system control software. If all the settings are correct and the image system is properly synchronized, image capturing is possible when the pulp flow system is operational and the refiner is rotating. The image capture is started by pressing the "capture" button on the "image capture" tab of PixeLINK image capture software shown in appendix 5.

9 PRELIMINARY TRIALS AND RESULTS

9.1 Pulp flow system and refiner testing

The pulp flow system was tested to determine the maximum operation consistency of the SBR station. The flow system was first tested with pulp consistencies from 0,5 % to 4 % with the original stator bar (gap size 700 μm) using long fibred softwood pine pulp. The result from these tests was that when operating at consistencies higher than 2 %, the refiner unit was at risk of clogging from the pulp suspension. Also the rotor would occasionally get jammed due to the build up of pulp on the edges of the rotor bars when the flow system and refiner were stopped. This was probably caused by the fact that the refiner unit was installed higher than the storage tank which leads to the draining of pulp suspension from the refiner unit. Pulp concentration inside the refiner chamber increases which can jam the rotor when refiner is started again.

The refiner unit is driven by an electric motor equipped with a frequency converter for adjusting the rotational speed of the rotor. Because the scale of the converter adjustment was 0 – 100 %, a digital tachometer was used to measure the corresponding Revolutions per Minute values from the refiner rotor shaft. The results are presented in Table 4. Figure 46 describes the linear relationship between motor power and RPM values. These values are applicable to pulp consistencies ≤ 2 %.

Table 4. Measured refiner rotor RPM values.

P (%)	0	10	20	30	40	50	60	70	80	90	100
RPM	0	38	79	118	157	196	235	274	313	352	391

Refiner RPM as a function of motor power
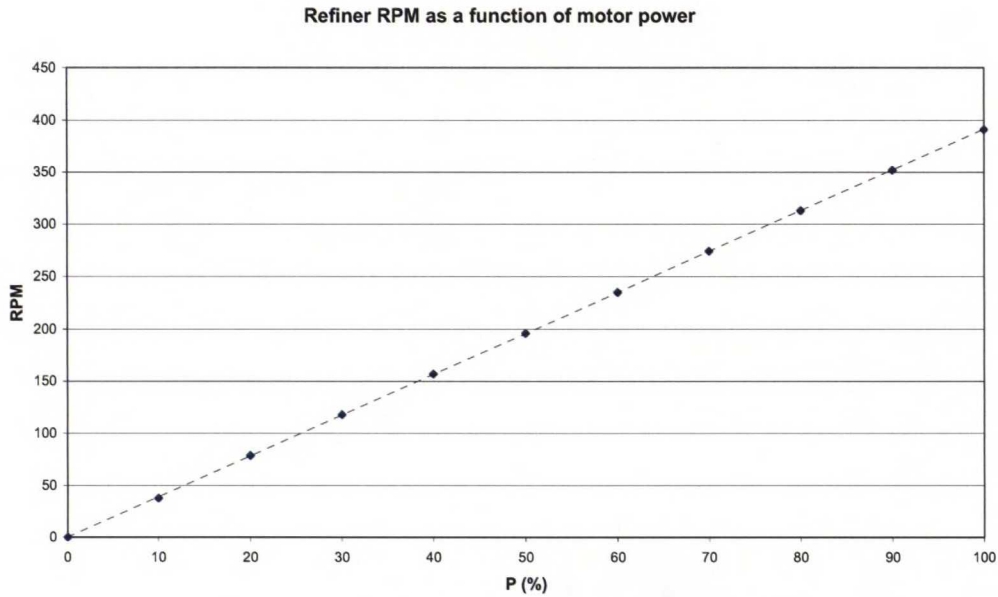
Figure 46. Single Bar Refiner RPM values as a function of the adjusted motor power.

An equation to calculate RPM value from adjusted motor power was created with Microsoft Excel© software from the chart presented in Figure 46:

$$RPM = 3,92P + 0,14, \tag{25}$$

where

P is   adjusted motor power [%].

The preliminary trials were concentrated mostly on testing the operation and basic functions of the SBR station. These included also testing the limits of the pulp flow system to define the maximum operating consistency of the refiner. There were not any unexpected problems during the testing of basic operation of the SBR station, but the results indicate that the flow system should not be operated with pulp suspensions that have higher consistency than 2 %. However if a solution to prevent the clogging of pulp suspension inside the refiner unit is discovered, it may be possible to use higher consistency pulps. It should be noted that only long fibred softwood pulp (pine) was used in the preliminary trials, so results can be different if short fibred hardwood pulp is used.

9.2 Measuring the amount of pulp in the refiner gap

An idea for experimental method for measuring the exact amount of pulp between the refiner bars was preliminary tested. The first phase of the measurement was to turn the pulp flow system on but not starting the refiner. Instead, the refiner rotor was turned by hand and stopped in the position where the stator and rotor bars are aligned. After this the flow system was stopped and the refiner unit was drained from pulp, which left only the flocs of fibres trapped inside the refiner gap. This pulp was then scraped off from the surface of the rotor bar by hand and weighed after drying it for 24 hours in a temperature of 105 °C. This procedure was then used to measure 12 samples using 150 μm gap size and pine pulp with a consistency of 2 %. The pulp mass per bar length and consistency in the gap was also calculated by using the bar dimensions given earlier. Results from these measurements are presented in Table 5.

Table 5. The results from pulp weight measurements.

sample	m (pulp,g)	m/bar length (kg/m)	c in gap (%)
1	0,0262	4,23E-04	78,26
2	0,0080	1,29E-04	23,89
3	0,0100	1,61E-04	29,87
4	0,0160	2,58E-04	47,79
5	0,0211	3,40E-04	63,02
6	0,0287	4,63E-04	85,72
7	0,0229	3,69E-04	68,40
8	0,0483	7,79E-04	144,27
9	0,0165	2,66E-04	49,28
10	0,0313	5,05E-04	93,49
11	0,0122	1,97E-04	36,44
12	0,0296	4,77E-04	88,41
Average	**0,0226**	**3,64E-04**	**67,40**
95 % conf.	0,0064	1,03E-04	19,06

These results are only indicative and much larger amount of measuring points would be required in order to get any reliable data. The process of measuring a single sample is very time consuming and laborious, so measuring larger amounts would require lot of time and effort. Also the amount of pulp that was weighed was partly originated from outside the actual refining gap because some of the flocs trapped between bars would be only partly inside the gap. This makes the amount of pulp larger than it should be. But this type of "hands-on" measurement

is perhaps the only way to know the exact amount of the pulp inside the gap so further development of this kind of technique could be considered in the future.

9.3 Imaging system testing

The imaging system testing included trial runs and digital image analysis of pictures that were captured from inside the refiner gap during surface-to-surface phase of the refining. The target of this trial was to study the correlation between the average pixel brightness values of analyzed images and the consistency of the refined pulp suspension. The average brightness value was expected to indicate the amount and coverage of the fibres along the bar surface because of the light refraction from the fibres. The imaging system was tested by first setting up the equipment and capturing images from inside the refiner gap during surface-to-surface phase of the refining event. The tests were conducted using pine pulp at five consistencies from 0,4 % to 2,0 % and using three different gap sizes of 150 μm, 300 μm and the original 700 μm. 100 images per each test point were captured to increase the reliability of the test. One of the captured images is shown in Figure 47. The region highlighted with the white rectangle is the analyzed area between the stator and rotor bar surfaces where bundles of fibres and flocs are receiving refining treatment.
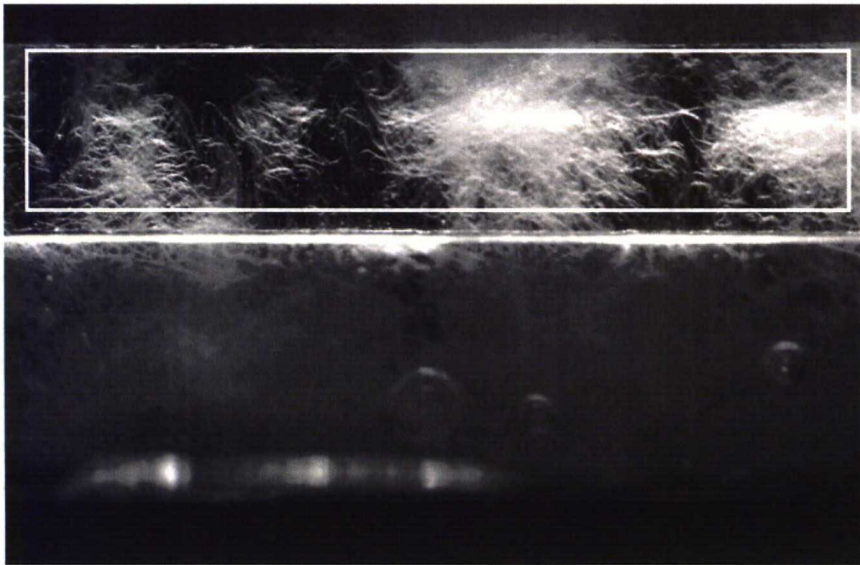
Figure 47. An image captured from inside the refiner gap. Pine pulp at 1,6 % consistency, gap size 150 μm, rotation speed 196 RPM. Analyzed region is highlighted with white rectangle.

Figure 48 shows a series of example pictures taken when using different gap sizes and pulp consistencies.
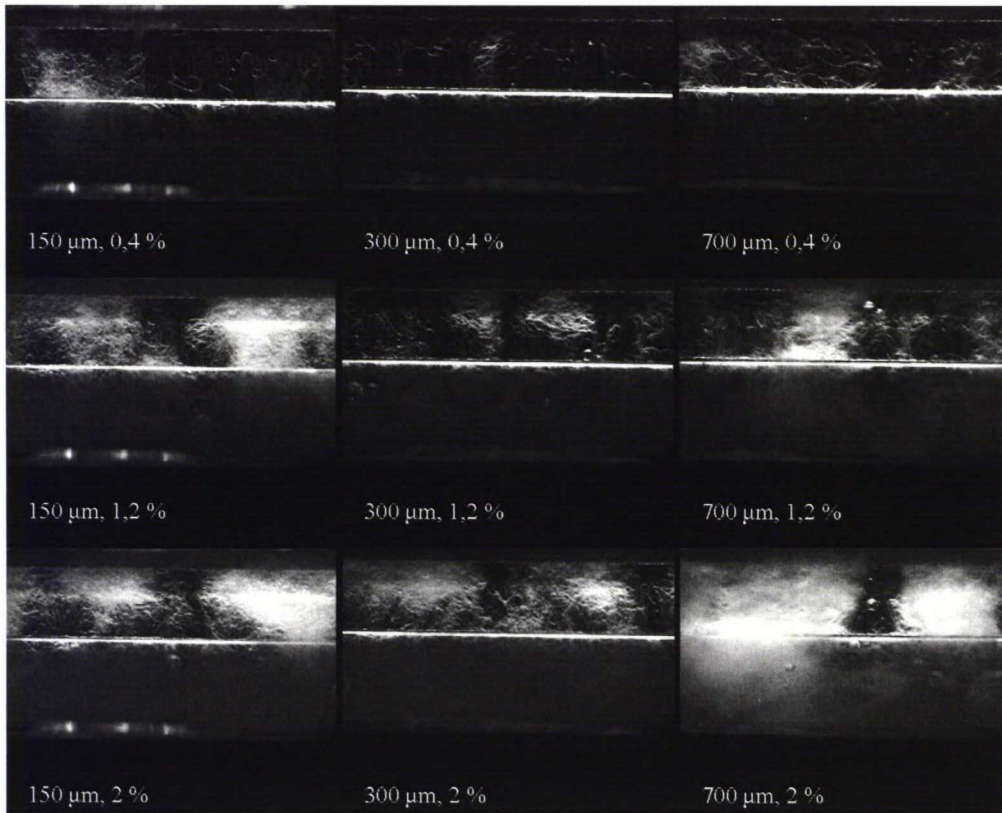
Figure 48. Pictures taken from the refining gap, variable gap size and pulp consistency, rotation speed 196 RPM.

The images that were captured are sharp enough to clearly recognize flocs, bundles of fibres and even individual fibres in the refining zone. Difference in the behavior of the fibres can be seen when the refined pulp consistency increases. Also the gap size seems to be affecting the amount of pulp and composition of the fibre flocs in the gap. It also seems that even at the most realistic conditions (150 µm gap size, 2 % consistency) the bar is not fully covered with fibres.

9.4 Image analysis

Analyzing of the captured images was made by using Matlab© mathematical analyzing software. A brightness value was defined for each pixel of every image captured. Because the resolution of the images was 8 bits, every pixel would have a brightness value between $0 - 255$ ($2^8 = 256$). The average pixel brightness value of each picture in a test point was calculated and the results are presented in Figure 49 and Table 6 along with R^2 values describing the correlation between

consistency of the refined pulp and the average pixel brightness values. Appendix 6 contains the measured values for each test point.

Figure 49. The average brightness values of the captured images as a function of pulp consistency and gap size.

Table 6. The results of the average pixel brightness calculations and correlations.
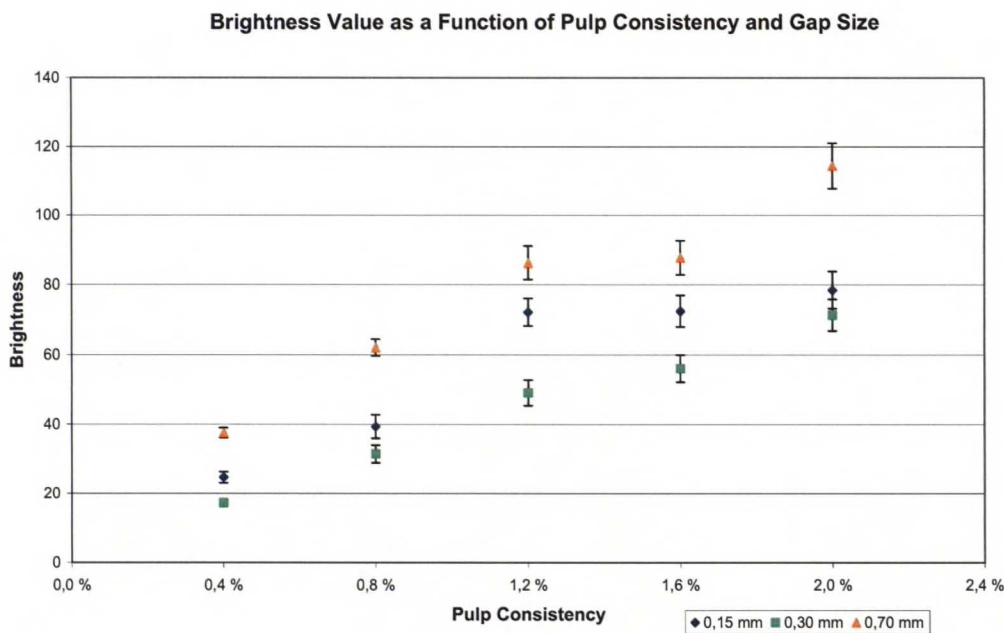
Gap size	Consistency	Brightness	95% conf.	R² value
0,15 mm	0,4 %	24,65	1,61	0,953
	0,8 %	39,37	3,39	
	1,2 %	72,20	3,90	
	1,6 %	72,53	4,48	
	2,0 %	78,50	5,29	
0,30 mm	0,4 %	17,21	0,38	0,987
	0,8 %	31,43	2,55	
	1,2 %	49,11	3,71	
	1,6 %	56,10	3,91	
	2,0 %	71,37	4,49	
0,70 mm	0,4 %	37,59	1,41	0,866
	0,8 %	62,09	2,38	
	1,2 %	86,25	4,80	
	1,6 %	87,74	4,89	
	2,0 %	114,44	6,63	

The results show that with all gap sizes, increasing the consistency of the refined pulp suspension increases the average pixel brightness value almost linearly. This means that when refined pulp consistency increases, more fibres and flocs are trapped between the stator and rotor bar surfaces. An interesting result is that average pixel brightness decreases when moving from 150 μm to 300 μm, but is at highest value when using the original 700 μm gap size. This would indicate that more pulp is simply flowing through the gap when using the original gap size compared to the more realistic smaller gap sizes where pulp has to be "captured" by the rotor edge in the gap. These results give some indication about the behavior of the consistency inside the refiner gap, but more research is needed in order to get any exact quantitative data and to link the brightness values to the consistency of the pulp inside the gap.

10 RECOMMENDED NEXT STEPS

There are some proposals for future work with the Single Bar Refiner. The preliminary testing should be continued with different types of pulps (e.g. hardwood pulps) with higher consistencies to correspond with industrial scale low-consistency refiners (c $\geq$ 3 %). The SBR station could also be upgraded with measuring equipment to determine process conditions such as temperature or pulp flow rate if monitoring or controlling these variables is considered necessary in the future. A possibility to install a force sensor to be able to measure normal force acting on the fibres in the refining gap should be studied thoroughly to increase the understanding of refining forces leading to fibre deformation. The measurement of normal force in connection with knowledge of the amount of pulp in the gap would enable greatly improved analysis of forces affecting fibres.

The image analysis with its possibilities and limitations is also a potential area of future research. Only preliminary trials with pine pulps and different refining gap sizes were conducted to test the suitability of this type of image analysis for measuring the pulp consistency inside the gap during surface-to-surface phase of the refining phenomenon. The results from these trials indicate that there is a strong correlation between pulp consistency and average pixel brightness values, but to be able to determine the exact consistency of the pulp inside the gap would require some kind of calibration of the imaging system. Developing the tested measurement method for defining the amount of pulp inside the gap could be one possible solution for the calibration problem. One target of this thesis was also to enable calculation of the fractional bar coverage in the refiner gap. This could be possible by using image analysis, but a suitable mathematical analysis method should be developed first.

11 CONCLUSIONS

The target of this thesis work was to construct a laboratory scale low-consistency refiner by modifying an existing design to enable more realistic refining conditions. The aim of the modification is to be able to study the refining forces and phenomena more closely. The designing and construction of a pulp flow system for the refiner unit was also an important part of the thesis. Also the setup and testing of a system for imaging fibres in the refining gap was realized.

The modification of the original design was made by designing a new stator bar with a groove in it. The purpose of this groove was to create more realistic conditions during refining. This design was first tested with the original stator bar by machining a groove in it similar to the one in the rotor bar, and later constructing two additional bars to reach the desired smaller gap size. The pulp flow system was designed and constructed to enable even flow conditions for the refiner unit. The installing and setup of the laser illuminated imaging system was conducted to enable image capture of the refining phenomena.

Some problems were encountered during the modification of the stator bars. The errors in measuring the original gap size resulted in wrong dimensioning of the new stator parts. For this reason some modifications had to be made afterwards to reach the targeted gap sizes. The pulp flow system was constructed without any major issues, but problems with the refiner unit clogging when operating with pulp consistencies > 2 % left some room for improvement. The imaging system installation and preliminary trials were successful, resulting in some good images from the gap between the rotor and stator bars. Images showed e.g. that bar coverage is clearly not 100 % at 2 % refining consistency, and that there is potential in developing the image analysis method aiming to determine bar coverage and pulp consistency in the gap. Many problems were solved during this thesis but many questions are still unanswered. These include the installation of a force sensor for measurement of normal force in the refiner gap and the development of image

analysis for further research. The target of the thesis work to construct a research tool for refining studies was achieved.

LIST OF REFERENCES

1. Lundin, T. Tailoring Pulp Fiber Properties in Low Consistency Refining. Doctoral Thesis. Åbo Akademi University. Laboratory of Fibre and Cellulose Technology. Turku 2008. 259 p. + Appendices.

2. Hiltunen, E. On the Beating of Reinforcement Pulp. Doctoral Thesis. Helsinki University of Technology. Laboratory of Paper Technology. Espoo 2003. 65 p. + Publications.

3. El-Sharkawy, K. Different Approaches to Tailoring Chemical Pulp Fibres. Doctoral Thesis. Helsinki University of Technology. Laboratory of Paper Technology. Espoo 2008. 58 p. + Publications.

4. El-Sharkawy, K. ENGINE-report SB 1, Final. Helsinki University of Technology, Paper and Printing Technology Research and Education Group. Unpublished document. 2008. 22p. + Appendices.

5. Pearson, A. J. A Unified Theory of Refining. Joint Textbook Committee of Refining. Series No.6. Montreal 1990. 128 p.

6. Solitander, A. Kaksikymmentä luentoa paperin tuntemuksessa – Apukirja kaikille kirja- ja paperin jalostusteollisuudessa työskenteleville. Isak Julinin kirjapaino. Tampere 1912. 152 p.

7. Lumiainen, J. Refining of Chemical Pulp. Papermaking Part 1, Stock Preparation and Wet End. Ed. Hannu Paulapuro. Publ. Fapet Oy. Helsinki 2000. pp. 86-122.

8. Kerekes, R. J. Characterising Refining Action in PFI-mills. 6th Pira International Refining Conference. Toronto 2001. Paper 11.

9. Koskenhely, K. Effect of Selected Filling and Pulp Suspension Variables in Improving the Performance of Low-consistency Refining. Doctoral Thesis. Helsinki University of Technology. Laboratory of Paper and Printing Technology. Espoo 2007. 49 p. + Publications.

10. Batchelor, W. Lundin, T. Fardim, P. A Method to Estimate Fiber Trapping in Low-consistency Refining. Tappi J. 5 (2006):8. pp. 31-36.

11. Koskenhely, K. Refining of Chemical Pulp Fibres. Papermaking Part 1, Stock Preparation and Wet End, Totally Updated. Ed. Hannu Paulapuro. Publ. Finnish Paper Engineer's Association. Helsinki 2007. pp. 92-139.

12. Fahey, M. D. Mechanical Treatment of Chemical Pulps. Tappi 53 (1970):11. pp. 2050-2064.

13. Hietanen, S. Ebeling, K. A New Hypothesis for the Mechanics of Refining. Pap. Puu 72 (1990):2. pp. 172-179.

14. Page, D. The Beating of Chemical Pulps – The Action and the Effects. 9th Fundamental Research Symposium (Fundamentals of Papermaking). Cam-

bridge, UK. Sept 17-22 1989. Mechanical Engineering Publications Ltd 1989. Vol. 1 pp. 1-38.

15. Giertz, H. W. The Influence of Beating on Individual fibers and the Causal Effects on Paper Properties. International Symposium on Fundamental Concepts of Refining. Appleton. Sept 16-18 1980. TAPPI Press 1980. pp. 87-92.

16. McIntosh, D. C. The Effect of Refining on the Structure of the Fibre Wall. Tappi 50 (1967):10. pp. 482-489.

17. Retulainen, E. Niskanen, K. Nilsen, N. Fibers and bonds. Paper Physics. Ed. Kaarlo Niskanen. Publ. Fapet Oy. Helsinki 1998. pp. 54-87.

18. Seth, R. S. Zero-span Tensile Strength of papermaking fibres. Pap. Puu 83 (2001):8. pp. 597-604.

19. Jagenberg, F. Das Holländergeschirr in Briefen an einen Papiermacher. 1887.

20. Brecht, W. A Method for Comparative Evaluation of Bar-equipped Beating Devices. Tappi 50 (1967):8. pp. 40A-44A.

21. Wultsch, F., Flucher, W. Der Escher-Wyss-Kleinrefeiner als Standard-Prufgerät für Moderne Stoffaufbereitungsanlagen. Papier 12 (1958):13/14. pp. 334-342.

22. Brecht, W. Siewert, W. H. Zur Theoretisch-technischen Beurteilung des Mahlprozesses Modern Mahlmaschinen. Papier 20 (1966):1. pp. 4-13.

23. Meltzer, F. P. Technologie der Zellstoffmahlung. Doctoral Thesis. RWTH Aachen University. Aachen, Germany 1994. 148p.

24. Roux, J-C. Bloch, J-F. Nortier, P. A Kinetic Model for Pulp Refining, Including the Angular Parameters of the Equipment. Appita J. 60 (2007):1 pp. 29-34.

25. Lumiainen, J. A New Approach to the Critical Factors Effecting Refining Intensity and Refining Result in Low-consistency Refining. Papermakers Conference. Atlanta, USA. April 23-25 1990. Tappi press 1990. pp. 269-278.

26. Musselman, R. Letarte, D. Simard, R. Third Stage Low Consistency Refining of TMP for Energy Savings and Quality Enhancement. 4th Pira International Refining Conference. Fiuggu 1997. Leatherhead, UK 1997. pp. 141-147.

27. Hietanen, S. Ebeling, K. Fundamental Aspects of the Refining Process. Pap. Puu 72 (1990):2. pp. 158-170.

28. Lewis, J. Danforth, D. W. Stock Preparation Analysis. Tappi J. 45 (1962):3. pp.185-188.

29. Kerekes, R. J. Characterization of Pulp Refiners by a C-factor. Nord. Pulp Pap. Res. J. 5 (1990):1. pp. 3-8.

30. Hiltunen, E. Helsinki University of Technology. Personal communications. 2.7.2009.

31. Kerekes, R. J. Senger, J. J. Characterizing Refining Action in Low Consistency Refiners by Forces on Fibres. J. Pulp Paper Sci. 32 (2006):1. pp.1-8.

32. Kerekes, R. J. Energy and Forces in Refining. Hannu Paulapuro Symposium. Espoo, March 20, 2009. pp. 10-18.

33. Martinez, M. Kerekes R. J. Forces on Fibers in low-consistency Refining. Tappi J. 77 (1994):12. pp. 119-123.

34. Martinez, D. M. Batchelor, W. J. Kerekes, R. J. Ouellet, D. Forces on Fibres in Low-Consistency Refining: Normal Force. J. Pulp Pap. Sci. 23 (1997):1. J10.

35. Batchelor, W. J. Martinez, D. M. Kerekes, R. J. Ouellet, D. Forces on Fibres in Low-Consistency Refining: Shear Force. J. Pulp Pap. Sci. 23 (1997):1. J40.

36. Prairie, B. Wild, P. Byrnes, P. Olender, D. Frncis, W. Ouellet, D. Forces During Bar-Passing Events in Low-Consistency Refining: Distributions and Relationships to Specific Edge Load. J. Pulp Pap. Sci. 34 (2008):1. pp. 1-8.

37. Lumiainen, J. Refining Intensity at Low Consistency – Critical Factors. Pap. Technol. 32 (1991):11. pp. 22-26.

38. Stationwala, M. I. Atack D. Karnis, A. J. Distribution and Motion of Pulp Fibres on Refiner Bar Surface. J. Pulp Pap. Sci. 18 (1992):4. J131.

39. Demler C. L. Another Attempt at Refining Visualization. TAPPI 1994 Papermakers Conference. San Francisco, CA. April 24-27, 1994. TAPPI Press. Atlanta 1994. pp. 104-114.

40. Alahautala, T. Lassila, E. Hernberg, R. Härkönen, E. Vuorio, P. Optical Measurement of Pulp Quantity in a Rotating Disc Refiner. Meas. Sci. Technol. 15 (2004). pp. 2256-2262.

41. Anon. PL-A741 Machine Vision Camera System Guide. Pixelink. 2003. 48 p.

APPENDIX 1

Figure 50. The dimensions of the stator bar acrylic part for 300 μm gap size.

Figure 51. The dimensions of the stator bar stainless steel part for 300 μm gap size.
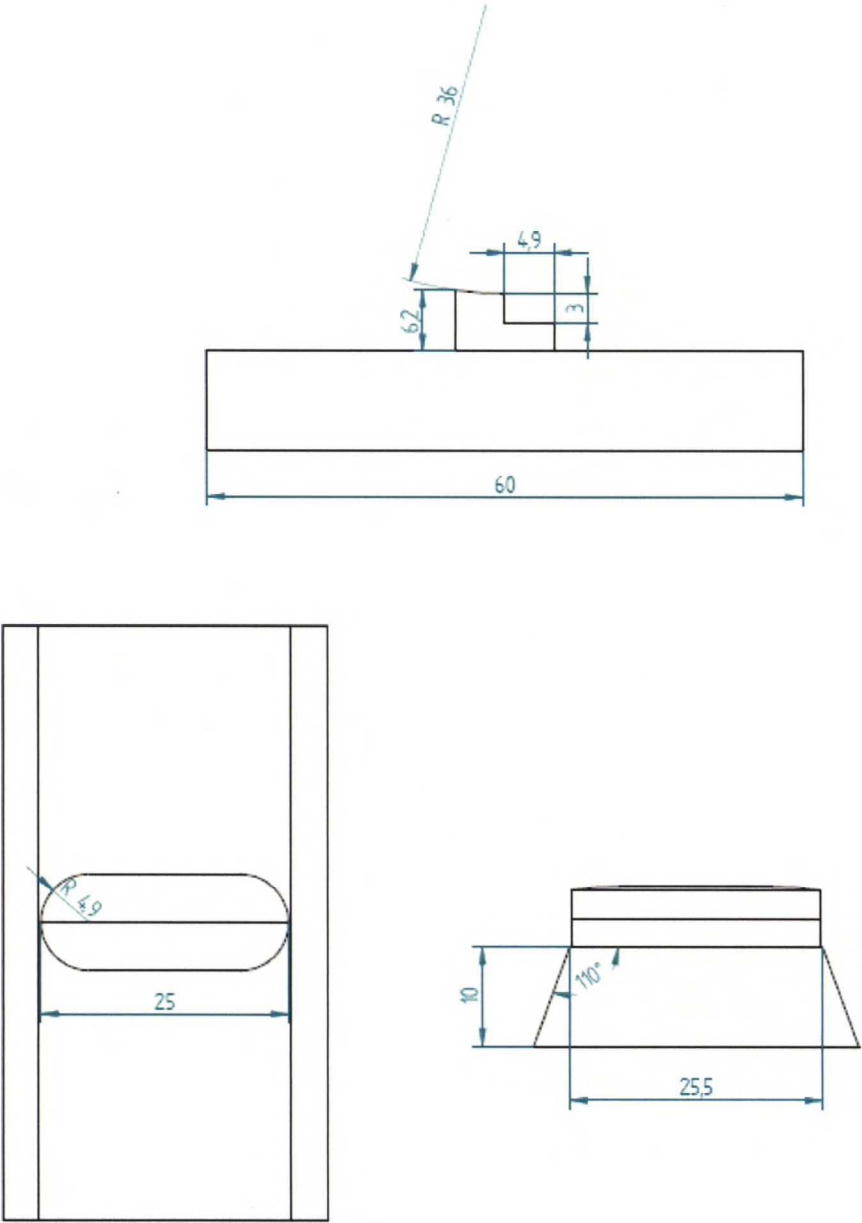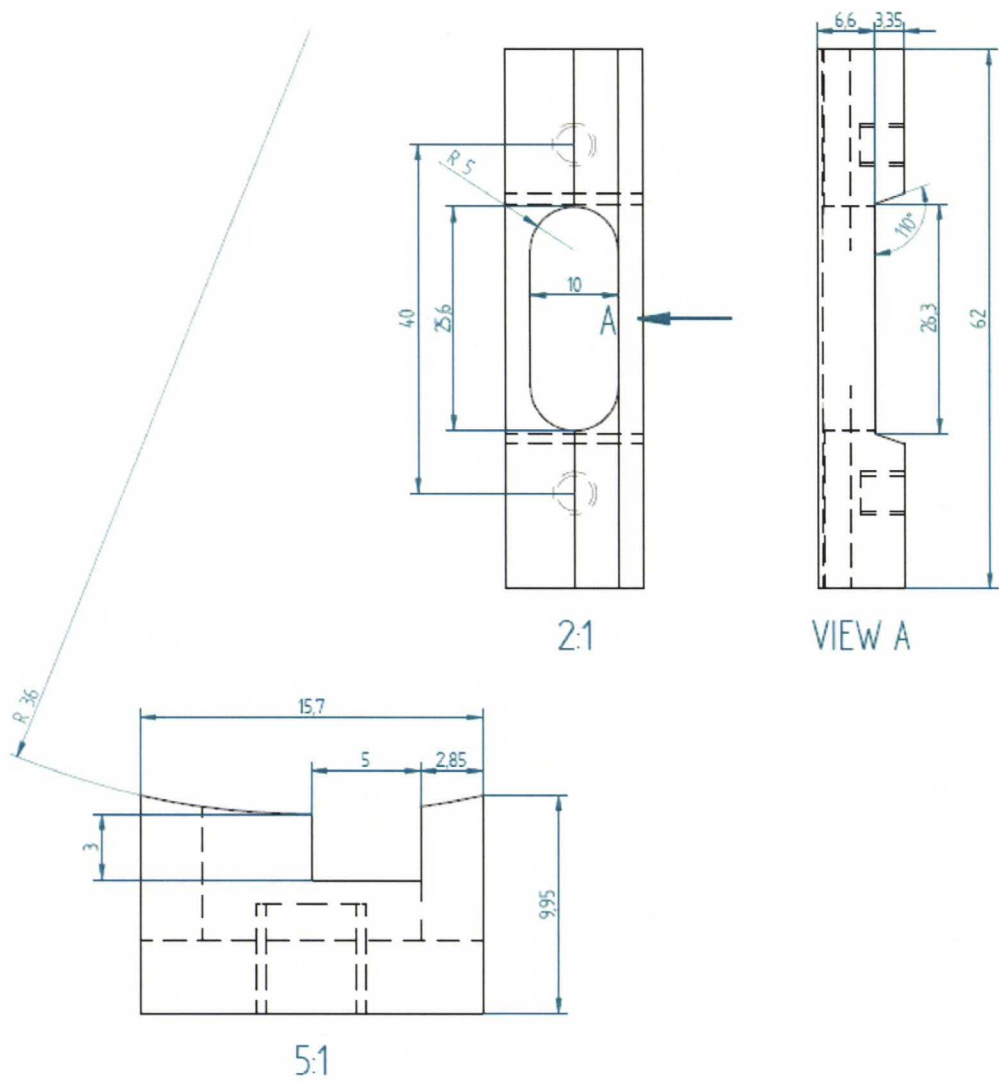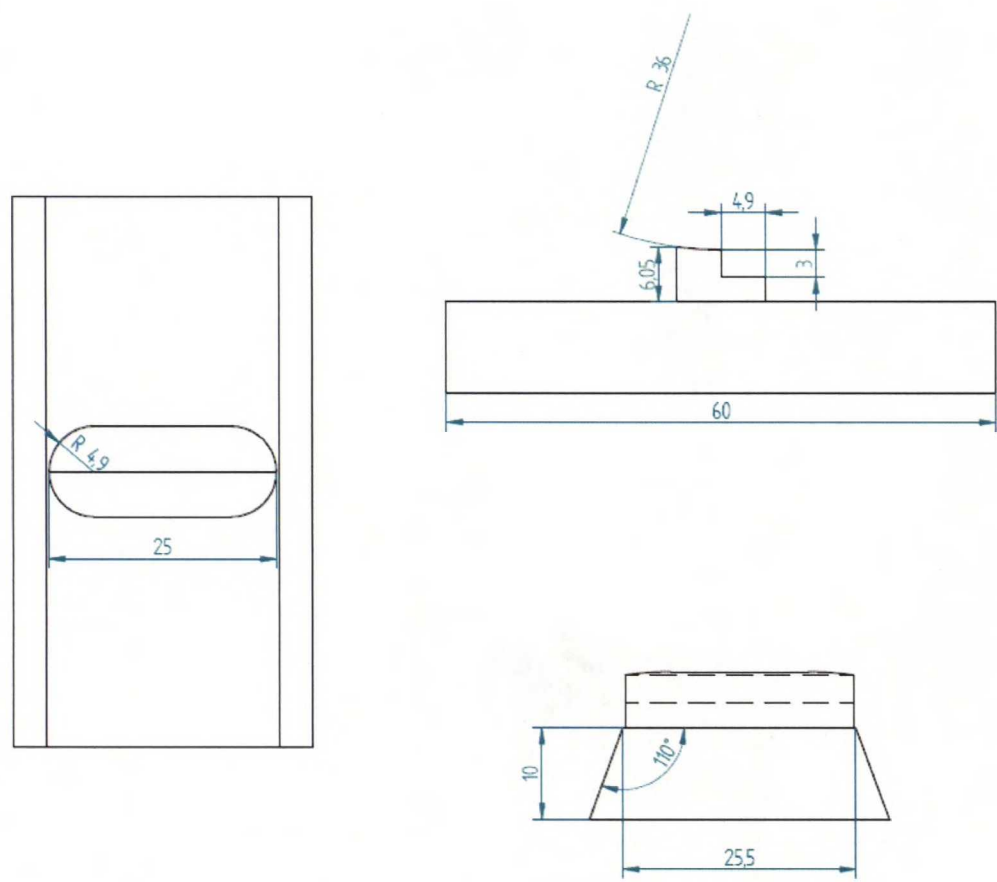
Figure 52. The dimensions of the stator bar acrylic part for 150 μm gap size.
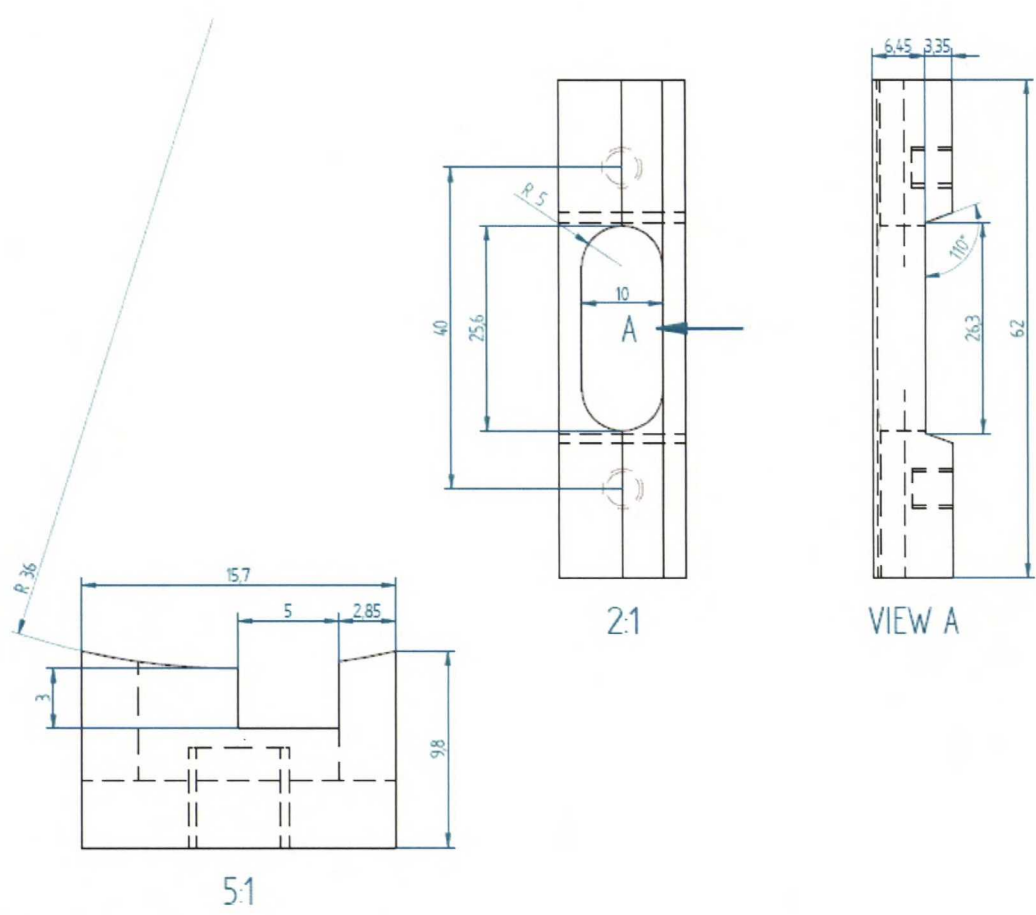
APPENDIX 4

Figure 53. The dimensions of the stator bar stainless steel part for 150 μm gap size.
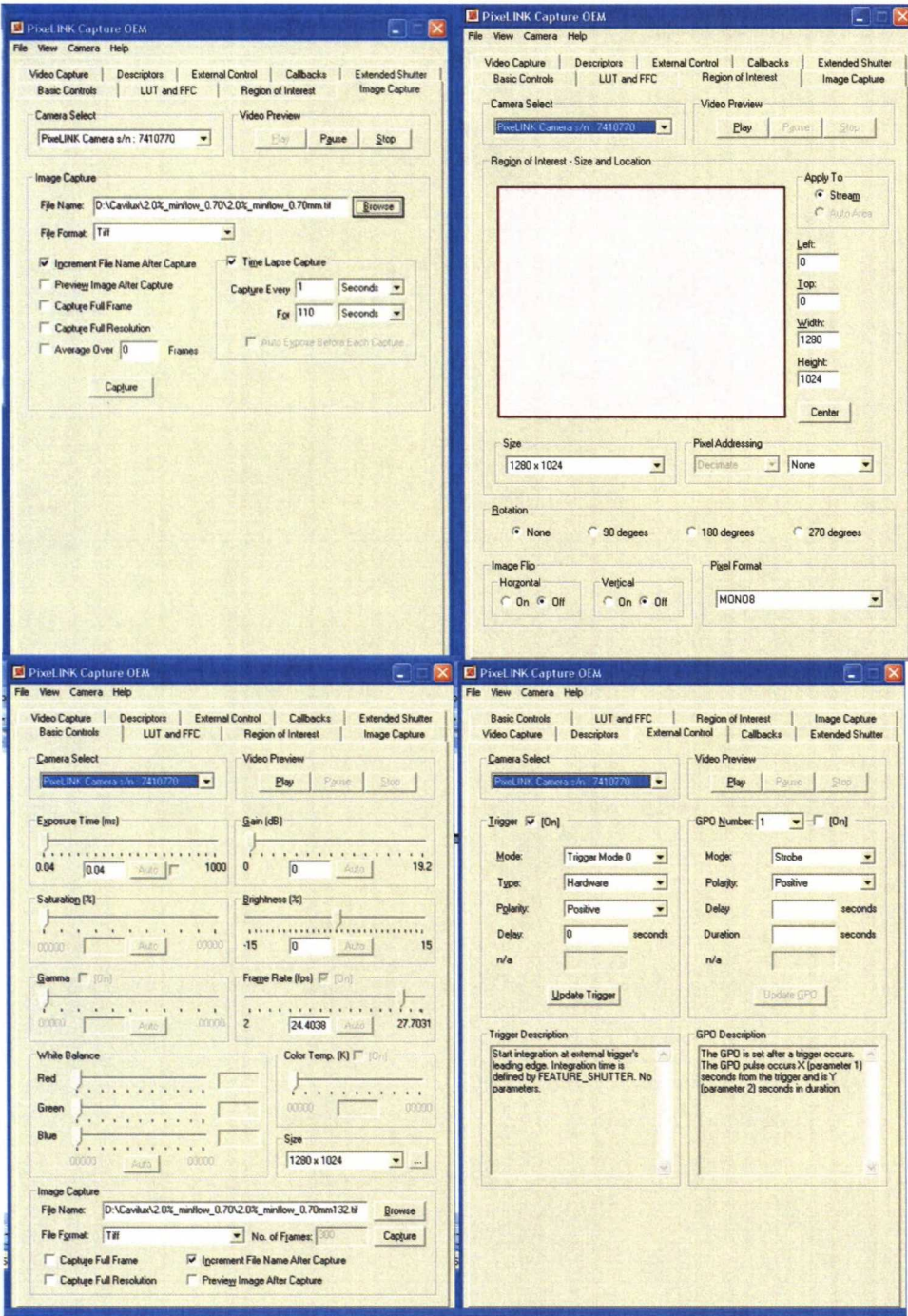
APPENDIX 5

Figure 54. The tabs of the Pixelink image capture software showing the settings used in preliminary trials.

Table 7. The average pixel brightness results from image analysis.

	0,4 %			0,8 %			1,2 %		
	0,15 mm	0,30 mm	0,70 mm	0,15 mm	0,30 mm	0,70 mm	0,15 mm	0,30 mm	0,70 mm
1	18,4671	14,6583	46,4924	52,8593	23,1802	73,2257	95,2917	46,5334	74,9988
2	46,1522	16,5137	39,1577	32,8667	19,6299	65,5569	63,3541	66,8901	86,5314
3	17,2499	15,7651	41,0043	52,8458	21,8449	43,2245	112,291	64,7512	83,2728
4	23,9393	18,502	46,8809	34,6642	28,247	59,7557	47,6363	74,8213	84,8423
5	16,9035	17,3853	43,2112	39,7378	41,6838	56,2312	51,156	101,594	57,1351
6	19,8157	17,135	41,9486	29,9001	23,2913	78,39	92,4515	62,2255	75,7671
7	37,9607	20,1749	39,7542	34,1154	61,1682	67,9276	77,007	68,4228	69,03
8	23,7883	16,4256	57,2094	40,3219	90,4959	55,4863	69,2142	98,1419	42,1779
9	21,4796	16,8659	48,5029	30,29	42,4811	45,0644	93,0248	42,349	117,107
10	17,8196	16,6985	35,8507	19,245	42,1557	62,8862	80,5268	40,5781	81,8841
11	29,3828	17,2615	27,2169	62,5449	26,3868	52,014	38,6498	43,8479	51,3717
12	20,4209	17,7211	33,5723	22,3366	29,806	67,0363	83,7904	50,5393	71,1963
13	20,2541	18,6761	43,5812	24,2859	24,6122	48,0976	118,222	39,8477	83,8975
14	26,7701	18,1675	34,3111	28,1325	23,8885	68,9129	68,583	41,5229	62,4671
15	20,7713	16,8282	37,143	51,6007	70,2545	65,7618	89,6427	48,6176	61,9187
16	25,7082	17,2398	40,5712	29,8294	59,3497	56,9572	71,1235	58,7974	68,8707
17	24,8199	16,0989	36,6854	30,5958	33,0575	71,3489	71,7712	39,3	94,6858
18	21,6247	15,609	44,1376	29,8157	21,881	58,0724	57,623	43,6825	91,7353
19	19,2822	15,7463	36,5529	37,1541	26,7187	79,8469	70,7692	50,4204	103,681
20	42,7023	15,3454	31,7341	33,099	17,7134	46,7317	76,0418	42,8565	84,2557
21	23,4693	17,2295	31,727	22,8366	23,4813	51,8055	82,8449	29,2789	43,4229
22	38,3874	15,1605	29,9536	25,8827	26,2518	57,6637	70,6457	31,6413	80,4245
23	37,4011	15,0819	36,7857	27,893	43,4845	49,4618	49,9894	26,4507	51,0045
24	17,5307	16,1332	33,3947	22,961	22,0575	60,7011	89,4905	65,4707	98,6513
25	28,375	19,378	34,1964	35,4993	29,3222	44,5247	56,2635	61,7006	99,6503
26	18,6831	15,7429	31,6744	50,0241	19,3834	107,842	52,947	44,8928	82,2916
27	17,2659	15,4633	60,4934	22,7969	25,3771	66,1248	86,5486	26,7895	89,0157
28	23,5324	17,2945	56,096	25,3645	29,3836	52,1814	47,0057	75,0685	103,606
29	20,7115	17,0845	40,6612	29,1946	26,93	76,7276	33,2402	44,1377	110,762
30	28,0096	16,908	40,3726	89,9422	23,8766	64,1041	27,3496	49,4949	94,5332
31	21,3804	16,4185	33,8327	49,19	23,6961	68,3853	41,3461	29,4504	103,215
32	26,0883	17,1281	37,008	27,5897	22,981	66,0742	91,0177	34,9724	51,6272
33	18,7069	16,4403	43,4812	58,5315	19,6528	71,3127	66,7866	61,892	75,3851
34	20,0721	17,9866	34,8697	76,5409	23,0305	47,4215	64,2831	22,8664	64,4317
35	38,0802	15,5097	35,8406	92,5476	28,493	45,4589	83,7952	54,7363	79,7906
36	34,5061	16,6196	69,8929	43,4565	45,7105	54,487	85,9502	29,4265	118,515
37	17,2481	23,8073	29,1423	79,0135	23,3385	57,9159	54,9665	31,9249	76,4693
38	18,5155	16,9387	43,6001	66,7795	35,6173	49,8463	94,5065	32,3255	101,009
39	35,9434	16,5787	36,42	47,7885	69,7147	53,954	73,8566	43,5997	104,382
40	34,5649	21,1635	39,4396	20,9118	23,7442	44,0609	55,94	61,4262	79,4048
41	37,807	16,2642	26,8185	19,3724	56,5932	56,0365	96,3263	49,3093	82,5777
42	16,1261	15,3966	28,8648	36,5229	30,1763	47,8033	72,1165	26,9739	76,9414
43	17,2666	15,497	42,2802	26,2115	26,8994	60,4334	61,3428	40,6543	64,2285
44	23,7656	17,3748	41,815	23,9759	21,2762	59,7502	83,5123	33,6895	70,2288
45	19,9735	15,2018	34,8511	28,1614	23,1329	51,8552	91,6258	36,7532	100,191
46	21,6717	17,1591	38,2207	27,8222	36,5928	68,8106	68,5155	81,7236	112,704
47	19,2416	16,2043	33,3738	76,21	32,3547	57,4311	53,0632	69,6718	89,1261
48	17,1553	16,0664	35,3499	26,058	56,2738	61,2141	51,2175	26,6413	115,476
49	16,0724	20,0289	44,08	42,7456	30,5128	58,0233	78,2378	68,3503	62,8235
50	18,4291	21,1145	36,9313	30,589	19,4445	49,569	81,5044	25,9696	109,583
51	34,1368	14,913	25,1045	46,3596	20,5963	62,393	102,72	106,023	96,8941
52	38,1656	18,8704	33,9586	40,9019	33,43	71,1892	36,094	35,8872	80,8798
53	15,6043	15,3567	30,0198	29,1635	22,9628	48,9802	77,9699	32,7297	129,923
54	19,0315	17,6721	35,9583	51,9744	19,4876	86,9466	96,9637	38,6141	91,4054

55	30,9857	18,7532	28,9294	48,9011	27,9787	76,4237	68,9112	24,5281	67,6697
56	21,0706	17,247	34,99	64,9274	45,46	50,6324	88,7522	71,7384	70,2765
57	19,3784	15,8187	32,7018	25,3324	24,4817	54,2862	37,0819	41,1575	79,9008
58	18,7817	16,5161	35,4948	40,5862	32,313	66,7243	88,9574	65,8618	97,8404
59	41,2599	18,5105	34,1534	49,962	26,3984	63,6362	105,397	53,1151	82,4449
60	18,7043	16,5372	41,0723	19,5822	29,4053	76,6284	74,0159	28,9879	88,325
61	16,8405	18,5178	30,3978	21,7672	25,8582	82,5445	90,4828	62,5884	111,789
62	22,3503	18,5605	33,1691	50,1261	46,4565	74,6669	79,7888	75,6437	90,1422
63	17,7995	16,1682	35,2569	32,2258	48,6714	69,8758	54,6156	23,5117	93,3382
64	25,2699	17,0889	34,1598	44,2299	30,2802	65,3699	63,4594	61,5827	118,969
65	51,0841	17,9766	24,7753	61,1038	18,8775	61,4616	57,4231	56,6411	72,8532
66	22,5429	14,4499	34,5817	81,6474	30,4317	68,5241	70,2914	68,6399	123,582
67	18,7004	16,4754	32,4518	49,534	20,5035	98,5777	48,2843	31,8324	80,1767
68	22,0061	18,0457	36,9861	60,6047	36,266	75,7348	89,715	42,415	43,5573
69	32,9401	17,3648	41,6294	30,4047	27,1907	53,2716	52,3467	35,7642	140,929
70	18,9757	18,0131	34,8291	48,834	34,5716	54,1172	82,0263	36,2472	77,4927
71	16,916	23,1972	42,1679	56,9374	20,9013	55,6341	58,0726	66,3915	56,176
72	33,1646	15,4001	39,646	21,4726	20,2465	49,6829	104,018	61,5025	118,226
73	39,4834	12,6513	38,5028	29,6369	15,84	56,9545	55,7115	55,98	88,956
74	20,0648	16,459	39,5956	22,2911	26,2201	68,8686	99,7311	30,4379	56,9673
75	20,5822	14,8245	25,7086	33,6062	28,097	65,2479	54,5651	19,5018	64,1683
76	18,0634	16,3289	34,1674	49,6645	46,2496	66,5857	38,9498	20,9944	79,1351
77	17,6569	16,958	34,1667	62,7635	18,9995	54,2502	60,6663	48,4004	47,6206
78	32,5549	16,4402	30,4715	31,1567	39,5341	51,3554	72,9334	42,5803	106,562
79	18,8399	15,8827	28,0745	21,725	27,0539	52,2037	73,3846	63,4767	156,132
80	20,0409	18,2068	40,9409	25,5668	20,3652	52,8955	76,3421	53,2516	89,0537
81	19,468	18,7027	35,9239	56,7632	38,5458	64,8173	58,1782	37,8205	153,501
82	26,0674	18,0348	38,6725	27,0968	30,9372	63,285	73,7523	55,9125	93,9246
83	19,537	24,4111	29,2294	30,0512	26,6302	52,9932	43,8148	41,1151	128,234
84	28,5674	15,9922	34,1215	41,3287	27,128	80,5012	57,1895	48,27	95,375
85	19,3453	16,925	31,054	36,8354	22,1311	58,9325	103,718	68,1178	61,6447
86	18,7349	19,3961	36,3978	27,296	46,6347	53,0214	97,364	33,5675	75,34
87	16,8609	17,9106	36,713	19,2854	27,1599	78,9879	60,0242	89,3173	49,29
88	18,7161	16,6338	43,6573	20,7964	33,4823	52,4075	75,5513	69,8589	65,2469
89	24,4888	18,5751	41,6089	41,9982	22,3479	71,7774	77,2044	28,6235	65,0658
90	20,6738	21,3218	36,35	38,0598	30,9491	55,8462	68,7094	34,5868	96,2534
91	29,9764	17,6651	42,1202	33,0596	38,2357	64,4044	60,5563	43,0184	55,3131
92	32,2838	17,9677	30,8213	69,6435	24,5527	55,5395	101,981	51,6686	90,2039
93	25,412	15,1277	48,0526	76,7389	60,5441	60,5855	37,7525	38,9445	73,7635
94	34,9438	16,8967	46,2079	26,6136	34,8592	62,9293	99,6912	47,8247	168,07
95	17,8262	16,7272	37,4759	24,4012	44,1344	63,2929	105,781	23,8987	89,5939
96	30,5005	20,2884	43,7416	21,8364	28,9191	48,1582	83,5112	88,3156	69,2249
97	49,1306	17,5179	33,3036	23,3301	26,0496	90,1698	54,2185	22,8102	92,2755
98	17,3829	16,5739	42,6321	35,6477	24,1979	77,4663	95,3483	68,9544	64,5978
99	19,5188	14,0789	37,5501	22,5388	18,9964	84,867	57,9426	71,6586	91,899
100	31,0047	17,4767	41,86	42,2677	24,6044	49,7712	73,5694	48,0308	106,575
Avg	24,6473	17,2062	37,5854	39,3723	31,428	62,0892	72,1993	49,1136	86,2508

1,6 %			2,0 %		
0,15 mm	0,30 mm	0,70 mm	0,15 mm	0,30 mm	0,70 mm
76,2679	54,2314	102,472	60,6257	27,6717	77,8931
68,0199	48,9986	56,3189	116,037	66,4194	87,5048
110,58	47,7598	78,6097	80,4961	115,882	55,9314
86,9484	45,5791	76,876	86,7548	62,6138	122,254
72,5971	75,011	130,09	72,819	57,9322	156,76
59,8953	68,6169	72,6291	67,6037	70,2714	108,228
95,0469	53,448	71,6396	103,392	91,6777	118,744
66,831	75,6624	58,3118	63,1692	93,9644	115,356
101,946	58,818	127,343	68,3807	90,1779	150,813
67,1392	69,7204	49,9704	100,628	55,6954	83,5509
87,8518	65,4219	46,0089	99,7638	70,618	68,8197
57,6761	60,6323	97,6046	28,9226	105,675	161,512
76,7441	34,6701	100,005	92,9928	83,847	131,23
28,3898	45,1393	121,205	58,609	90,6764	143,148
100,756	76,5912	81,095	66,2577	54,4219	120,924
95,2687	84,7287	77,8459	113,888	68,6426	150,555
52,4645	29,8169	82,5504	97,7723	93,5386	159,586
77,0236	54,2102	81,9152	30,8531	91,8584	114,895
75,875	27,796	75,8241	78,3154	63,3902	67,3798
88,3038	61,6777	142,412	31,1697	97,1376	162,793
56,8981	38,7693	60,2007	63,218	83,2983	117,559
37,1288	66,2399	89,4768	66,232	55,0602	73,3693
79,7611	70,0805	117,84	118,798	59,7839	88,8489
39,1143	61,3491	79,1993	125,896	83,9736	107,532
115,213	39,2417	87,1935	96,4737	48,7205	80,0173
80,6888	33,4919	120,902	23,7433	43,3521	182,15
86,0728	55,0125	103,035	76,0936	28,9351	92,2025
67,0099	89,4436	77,9327	97,6996	64,9107	130,389
99,5479	70,9674	59,9794	62,0816	122,447	79,2537
57,2393	34,9773	101,462	84,3164	117,739	103,437
62,3022	75,1562	98,3526	73,7642	59,32	82,6472
112,389	74,4598	84,5399	74,3534	70,0295	131,91
68,2575	50,9266	57,6702	58,8526	66,5524	110,313
62,3524	69,7815	80,5675	71,8907	64,1714	88,6391
81,1248	21,6487	66,5843	76,5431	54,7656	111,457
123,717	67,9849	68,3868	120,029	74,61	197,177
71,5745	41,1732	78,7123	69,6946	69,6055	99,1083
93,6243	59,1721	68,4741	77,4633	87,0216	68,2486
68,4698	51,35	104,657	133,447	41,4822	102,371
76,6662	102,773	52,5639	28,8663	63,115	94,1852
37,1046	48,9694	111,307	106,367	120,1	74,9673
92,9548	30,2371	58,2788	113,602	57,4219	94,8641
88,2201	40,5338	68,2159	73,412	68,6465	121,436
60,6425	90,7264	116,883	88,3343	40,8249	160,442
97,9073	54,3316	67,8512	87,579	52,8622	123,113
67,7346	83,3861	67,0929	104,315	40,7009	165,803
43,0812	41,2891	65,6922	102,775	80,6446	101,011
55,1773	26,9823	71,0463	40,3583	37,4392	116,914
77,2396	93,3203	80,6109	97,0282	75,7777	104,93
99,6482	62,5926	87,9372	88,5158	130,58	62,7758
66,2683	33,5075	54,1472	60,6601	71,9701	173,913
54,0771	51,8481	51,4711	46,1243	81,7325	53,6952
61,4103	47,799	90,3052	71,8837	66,8016	117,627
66,286	35,2092	89,2722	99,4946	84,4962	170,61

46,1313	34,7046	92,8721	38,5715	63,8933	114,115
43,4471	85,5761	72,1481	36,0551	63,0922	146,706
44,3464	46,6345	75,5198	127,12	123,237	202,371
90,4822	40,9482	56,4321	61,4731	63,3925	88,9092
55,056	64,3319	67,0897	40,045	38,4166	107,907
105,535	33,7875	46,0692	59,4897	67,4827	135,118
83,8612	75,5993	112,712	62,6919	87,1898	60,0727
47,7996	33,1136	94,9513	92,6772	59,0854	174,468
75,7887	81,659	122,303	108,207	49,2341	139,451
35,8897	38,8096	91,3213	37,8465	95,5217	79,228
85,2863	51,2989	97,3269	94,4032	94,5396	115,698
63,1513	64,2598	122,086	91,2461	36,6122	124,88
52,0396	61,1354	68,4276	73,4983	71,314	151,674
112,917	34,0066	112,051	55,643	27,6294	105,169
60,0087	73,9141	104,391	79,109	56,3773	109,401
65,7575	63,8889	88,8867	73,6042	84,7503	92,7718
121,615	92,1114	69,7579	87,3621	55,407	86,41
77,8566	75,109	71,586	57,5726	74,4022	114,286
101,449	113,112	76,7226	70,4488	41,9381	95,1502
68,6254	60,7109	100,902	122,996	84,1864	84,0371
65,0346	64,7745	96,1242	149,755	97,6426	146,875
51,795	63,2432	116,479	108,652	54,2698	109,8
41,3256	36,8473	126,7	118,558	65,7757	148,798
71,5451	40,1561	167,776	89,5876	101,485	137,089
69,952	28,811	110,488	66,8222	58,582	107,75
133,381	42,4953	116,221	65,3009	99,8184	70,4682
74,2255	123,317	56,7751	30,0705	100,776	137,731
63,0131	67,0191	90,4888	52,704	93,7296	63,424
45,7561	25,0351	88,3273	81,171	67,9828	54,8
31,5374	74,0226	92,8329	79,9851	47,0198	99,8966
91,7204	35,9724	119,583	96,9474	49,1768	138,926
43,4863	62,6667	100,694	76,2962	57,7455	155,678
98,1745	28,7325	100,433	62,7363	78,8093	136,685
37,8413	55,2859	59,3459	87,1696	58,0567	151,727
46,6906	47,6452	151,596	87,8346	66,67	120,742
67,9638	65,6031	46,5913	137,911	65,8217	119,454
73,393	58,3663	56,569	81,7017	47,7982	60,3148
63,536	48,9485	71,4768	52,1357	82,9366	90,0955
93,1567	52,8638	88,5174	89,2332	75,2476	121,752
90,6595	42,263	67,0684	35,783	120,01	88,9175
111,013	34,9231	107,422	51,0342	29,7907	101,989
64,7605	43,6952	82,1222	48,7752	82,3479	137,88
83,9055	49,6696	99,0881	95,983	86,7869	177,594
34,3672	35,7475	115,08	93,5799	60,4899	89,5443
44,8704	46,3556	102,372	93,9571	78,8839	103,787
69,8591	57,3128	131,621	48,3169	50,6418	103,579
72,5254	**56,0975**	**87,7392**	**78,5042**	**71,37**	**114,439**

PKP - 10